

# Novel features of Spin Hall and Chern insulator phases realized by triplet excitations

Andreas Thomasen,<sup>1</sup> Karlo Penc,<sup>2</sup> Nic Shannon,<sup>1</sup> and Judit Romhányi<sup>1,3</sup>

<sup>1</sup>*Theory of Quantum Matter Unit, Okinawa Institute of Science and Technology Graduate University, Onna-son, Okinawa 904-0395, Japan*

<sup>2</sup>*Institute for Solid State Physics and Optics, Wigner Research Centre for Physics, H-1525 Budapest, P.O.B. 49, Hungary*

<sup>3</sup>*Department of Physics and Astronomy, University of California, Irvine, California 92697, USA*

(Dated: August 10, 2022)

The study of topological band structures has recently been extended from electrons to many other systems with band-like excitations. One promising avenue is the triplet excitations of quantum paramagnets, which can realize a variety of topologically–nontrivial band structures. Recently, triplet bands characterized by a  $\mathcal{Z}_2$  topological invariant, analogous to that introduced by Kane and Mele, have been discussed in a quantum paramagnet realized on a bilayer honeycomb lattice [D. G. Joshi and A. P. Schnyder, Phys. Rev. B 100, 020407 (2019)]. In this case, triplet bands from time-reversal (TR) partners, which play the role of the Kramers pairs of electrons in the Kane–Mele model. However, Bosonic triplet excitations do not enjoy the same symmetry–protection as Kramers pairs of electrons and can be mixed by interactions. The consequences of such mixing for the  $\mathcal{Z}_2$  topological phases of a quantum paramagnet remains an open question. In this paper, we explore this problem on the bilayer kagome lattice. We show that, as long as a  $\text{TR}\times\text{U}(1)$  symmetry is preserved, the triplet excitations provide a faithful analog of the Kane–Mele model. Kagome bands realize both a quadratic and a linear band touching, and we provide a thorough characterization of the Berry curvature associated with both cases. We also construct the most general TR invariant triplet Hamiltonian allowed by the symmetry. We find that exchange interactions with quadrupolar character, typical in realistic models, lift the required  $\text{U}(1)$  symmetry and destroy the  $\mathcal{Z}_2$  band topology. We further consider the effects of TR breaking by an applied magnetic field. In this case, the lifting of spin–degeneracy leads to the formation of a triplet Chern insulator, which is stable against the breaking of  $\text{U}(1)$  symmetry. We calculate the triplet–mediated spin Nernst and thermal Hall signals, making predictions, which could be compared with experiment.

PACS numbers:

## I. INTRODUCTION

The discovery, in 1980, of an integer quantization in the Hall response of a two–dimensional electron gas in high magnetic field<sup>1</sup>, marked a new beginning for condensed matter physics. It was quickly realised that this quantization implied a new form of universality<sup>2</sup>, enjoying protection against both interactions and disorder, with the quantized Hall response reflecting the integer values of the Chern indices characterising the topology of the underlying electron bands<sup>3–5</sup>. In a celebrated paper, Haldane noted that these conditions could also be met in a simple model of spinless electrons on a honeycomb lattice, with time–reversal symmetry broken by complex hopping integrals, but no magnetic field<sup>6</sup>. And the generalisation of Haldane’s model to spinful electrons, by Kane and Mele<sup>7,8</sup>, set the stage for the burgeoning field of topological insulators (TI’s) and superconductors<sup>9,10</sup>, with current estimates suggesting that as many as 27% of materials may have a topological band structure<sup>11</sup>. Moreover, since the exotic properties of TI’s follow from the single–particle properties of a band, analogous effects can also be found in a wide range of other systems, including photonic metastructures<sup>12,13</sup>, electronic circuits<sup>14</sup>, and both acoustic<sup>15</sup> and mechanical lattices<sup>16</sup>.

Another natural places to look for nontrivial topology is in the band-like integer spin excitations of insulating magnets. These may take the form of magnon (spin–wave) excitations of ordered phases, or triplet excitations of quantum paramagnets. Such excitations are Bosonic, and acquire Berry phases as a consequence of spin–orbit coupling, usually in the form of Dzyaloshniski–Moriya interactions<sup>17</sup>. As a result, both

magnon<sup>18–29</sup>, and triplon<sup>30–32</sup>, bands can exhibit non-trivial Chern indices, in direct analogue with TI’s<sup>33</sup>. These systems exhibit exactly the same topologically–protected edge modes as their electronic counterparts<sup>18,20,25,30</sup>, and can be indexed in the same way, even in the presence of disorder<sup>34,35</sup>. They also support thermal Hall<sup>19,21,25,30</sup> and spin–Nernst<sup>21,23–25,27,36</sup> effects, in correspondence to the Hall effect<sup>6</sup> and spin–Hall effects seen in electronic systems<sup>7,8</sup>.

However, since these topological bands are a feature of excitations, rather than of a ground state, the quantized Hall effect found in Chernful band of electrons<sup>3–5</sup>, is superseded by a non–integer, temperature–dependent response, coming from thermally–excited Bosons<sup>37,38</sup>. Moreover, the fact that interactions between Bosons can be relevant<sup>22,39</sup> also creates a new opportunities to study non–Hermitian aspects of their dynamics<sup>28,29</sup>.

Given the seminal role of the models of Haldane<sup>6</sup>, and Kane and Mele<sup>7,8</sup> in the understanding of electronic TI’s, it is natural to look for corresponding systems in magnets. The route to a Haldane model for magnons turns out to be both simple and elegant: the Heisenberg ferromagnet (FM) on a honeycomb lattice realises magnons with a graphene–like dispersion<sup>40</sup>, and the symmetry of this lattice permits DM interactions on second–neighbour bonds. These supply the complex hopping integral invoked by Haldane, opening a gap in the magnon dispersion, and endowing the bands with Chern numbers<sup>24,41</sup>. By extension, an exact analogue of the Kane–Mele model can be realised in a bilayer honeycomb magnet, with inter-layer interactions chosen such that it forms two copies of a Haldane model, with magnon bands related by time–reversal symmetry<sup>42</sup>, an approach which can be extended to the Fu–

Kane–Mele model in three dimensions<sup>43</sup>. And, it is also possible to achieve triplon bands which mirror the Kane–Mele model, in a quantum paramagnet on a bilayer honeycomb lattice<sup>32</sup>.

While the route to topological bands in magnets is now well established, a number of important questions remain. In particular, while  $S^z = \pm 1$  triplet excitations of a quantum paramagnet form a doublet under time–reversal symmetry, they do not satisfy Kramer’s theorem, and so are much more “fragile” than the electronic doublets considered by Kane and Mele. The consequences of any symmetry–allowed terms in the Hamiltonian which mix triplets with  $S^z = \pm 1$ , therefore need to be considered explicitly. It is also of interest to ask what such a topological quantum paramagnet would look like in experiment, and how this physics might generalise to structures more complicated than the honeycomb lattice. In this paper we explore the new features which arise within a model of a spin–1/2 Kagome bilayer, which provides a direct analogue of the  $\mathcal{Z}_2$  topological insulators considered by Kane and Mele<sup>7,8,44</sup>. We take a limit in which the ground state is a quantum paramagnet, formed by inter–layer dimers, with nine distinct bands of triplet excitations.

We consider first the case where the spin of triplet excitations is conserved, and show that in zero magnetic field the  $S^z = \pm 1$  triplons can realize an analogue to the Kramers pairs of the quantum spin Hall insulator<sup>7,44–46</sup>. In this case, triplon bands are characterized by a nonzero  $\mathcal{Z}_2$  invariant, and in open geometries we find corresponding helical triplet edge modes. Furthermore, when the time reversal symmetry is broken by applied magnetic field, the system evolves into a Chern insulator<sup>6</sup> characterized by chiral triplon edge modes appearing in a finite sample. We compute the spin Nernst, and thermal Hall responses marking the nontrivial topology in these phases.

We then explore the consequences of the spin–mixing terms allowed by the symmetry of the lattice, and discuss their effect on the  $\mathcal{Z}_2$  and Chern bands. Such spin–mixing terms are also present in the original model of Kane and Mele, in the form of the Rashba coupling<sup>7,8</sup>. In that case, the “up” and “down” spin states of an electron form a Kramers pair, enforcing the twofold degeneracy of the bands at certain points in the Brillouin zone. This guarantees the perturbative stability of spin–Hall state against small values of Rashba coupling. However such a protection is *not* guaranteed by time–reversal symmetry in the case of the triplons, where the representation of the time–reversal operator squares to one. We examine this difference closely, and find that even infinitesimal spin–mixing interactions can eliminate the  $\mathcal{Z}_2$  topological invariant, opening a gap to the associated helical edge modes. Because of the closely–related lattice symmetries, the main conclusions of this analysis are also valid for bilayer honeycomb model considered in Ref. 32.

The paper is organized as follows. In Section II we give a detailed analysis on the symmetry allowed intra-dimer and first neighbor inter-dimer interactions and introduce the bilayer kagome model. Sec. III is devoted to the Bogoliubov–de Gennes Hamiltonian describing the triplet dynamics, and provides a detailed discussion on the band touching topological transitions appearing as the anisotropies change. In Sec. VI

we show that the triplet excitations can provide an analog to the Kane and Mele model<sup>7</sup>, characterized by nonzero  $\mathcal{Z}_2$  topological invariant. We examine which terms compromise the triplet spin Hall state, showing the fragility of the  $\mathcal{Z}_2$  phase of a non-Kramers pairs. We calculate the Nernst effect of triplets, a transverse spin current arising as a response to a temperature gradient. In Sec. VIII we consider the time-reversal symmetry breaking case in the presence of magnetic field. We examine the stability of the triplet Chern bands. Additionally, we compute the thermal Hall signal of the Chern-ful triplon bands. Sec. IX provides a brief summary of our results.

## II. SYMMETRY-ALLOWED HAMILTONIAN

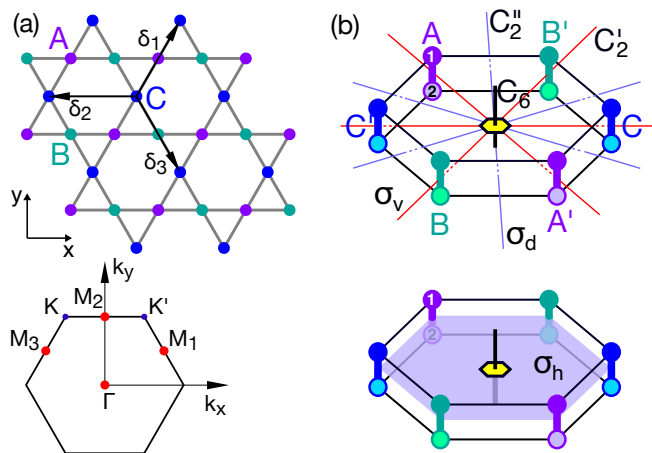


Figure 1: (a) Top view of the bilayer kagome lattice with the translation vectors,  $\delta_1 = (1/2, \sqrt{3}/2)$ ,  $\delta_2 = (-1, 0)$ , and  $\delta_3 = (1/2, -\sqrt{3}/2)$ . Bottom panel: Hexagonal Brillouin zone with time reversal invariant momenta (TRIM)  $\Gamma$ ,  $M_1$ ,  $M_2$ , and  $M_3$  (red), as well as the Dirac points  $K$ , and  $K'$  (blue). (b) Symmetry operations of the bilayer-kagome lattice. The smallest unit exhibiting the full symmetry of the bilayer kagome lattice is a bilayer hexagon with six inter-layer dimers. The indices  $A$ ,  $B$ , and  $C$  and following the notation of the main text corresponding to the orbital (sublattice) flavor, while the  $A'$  denotes the dimer  $A$  shifted with the lattice translation vector  $\delta_3$ ,  $B'$  is dimer  $B$  shifted with  $\delta_1$  and  $C'$  corresponds to dimer  $C$  translated by  $\delta_2$ .

The model we consider is the spin–1/2 magnet on the bilayer Kagome lattice, shown in Fig. 1(a). We first establish the most general form of first–neighbour and second–neighbour interactions allowed by the  $D_{6h}$  symmetry of this lattice. The resulting model,

$$\mathcal{H}_{D_{6h}}^{1,2} = \mathcal{H}_{XXZ} + \mathcal{H}_{DM} + \mathcal{H}_{Nematic}, \quad (1)$$

has fifteen adjustable parameters, and contains terms we which can group as symmetric XXZ exchanges respecting the  $U(1)$  symmetry (rotations around the  $z$  axes),  $\mathcal{H}_{XXZ}$ ; antisymmetric Dzyaloshinskii–Moriya (DM) interactions,  $\mathcal{H}_{DM}$ ; and symmetric diagonal and off diagonal exchange anisotropies

breaking the  $U(1)$  symmetry and which we name the "bond-nematic" interactions (defined below),  $\mathcal{H}_{\text{Nematic}}$ .

To determine the different contributions to Eq. (1), we consider the hexagonal prism formed by six interlayer spin-dimers [Fig. 1(b)], which forms the smallest building block with the full symmetry of lattice. In what follows, we refer to these interlayer dimers simply as "dimers", and we will ultimately build topological bands from the triplet excitations of a quantum paramagnet formed by singlets on these dimer bonds. The bilayer hexagon contains three such dimers A, B, and C that lie within the kagome unit cell, as well as three more, A', B', and C', which correspond to neighboring dimers translated by  $\delta_3$ ,  $\delta_1$ , and  $\delta_2$ , respectively [Fig. 1(a)].

We proceed by analysing all possible interactions bilinear in spins, starting from the transformation properties of individual spin components under three generators of the  $D_{6h}$  point group,  $C_6$ ,  $C'_2$ , and  $\sigma_h$  [Table I]. All remaining group elements can be constructed as a combinations of these three operations. The different types of term which arise are considered, bond by bond, below.

Table I: Transformation of the spin (axial vector) components, the dimers, and the site indices under the generators of the  $D_{6h}$  point group.

Generators	E	$C_6$	$C'_2$	$\sigma_h$
spin component	$S^x$	$\frac{1}{2}S^x + \frac{\sqrt{3}}{2}S^y$	$S^x$	$-S^x$
	$S^y$	$-\frac{\sqrt{3}}{2}S^x + \frac{1}{2}S^y$	$-S^y$	$-S^y$
	$S^z$	$S^z$	$-S^z$	$S^z$
dimer label	A	$C'$	B	A
	B	$A'$	A	B
	C	$B'$	C	C
	$A'$	C	$B'$	$A'$
	$B'$	A	$A'$	$B'$
	$C'$	B	$C'$	$C'$
site index	1	1	2	2
	2	2	1	1

### A. Intra-dimer interactions

The symmetry classification of the intra-dimer interactions according to the  $D_{6h}$  symmetry group yields three invariant terms. Two correspond to the Heisenberg exchange anisotropy distinguishing the in-plane and out-of-plane components

$$\mathcal{H}_{\text{XXZ}} = J_{\parallel} \sum_j (S_{j_1}^x S_{j_2}^x + S_{j_1}^y S_{j_2}^y) + J_{\perp} \sum_j S_{j_1}^z S_{j_2}^z. \quad (2)$$

The third intra-dimer term is a symmetric exchange anisotropy, which we refer to as the bond-nematic interaction:

$$\mathcal{H}_{\text{Nematic}}^{\bullet} = K_{\parallel} \sum_j \mathbf{n}_j \cdot \mathbf{Q}_{j_1, j_2}^{\parallel}. \quad (3)$$

The index  $j$  runs over the dimers, and 1 and 2 denote the site indices of dimer- $j$ . The vectors  $\mathbf{n}_j$  appearing in the nematic term have the form  $\mathbf{n}_A = \left(\frac{1}{2}, \frac{\sqrt{3}}{2}\right)$ ,  $\mathbf{n}_B = \left(\frac{1}{2}, -\frac{\sqrt{3}}{2}\right)$ , and  $\mathbf{n}_C = (-1, 0)$ , and  $\mathbf{Q}_{j_1, j_2}^{\parallel}$  denotes the vector  $(Q_{j_1, j_2}^{x^2-y^2}, Q_{j_1, j_2}^{xy})$  made of the nematic interactions

$$Q_{i,j}^{x^2-y^2} = S_i^x S_j^x - S_i^y S_j^y, \quad (4a)$$

$$Q_{i,j}^{xy} = S_i^x S_j^y + S_i^y S_j^x. \quad (4b)$$

We illustrate the nematic operators,  $Q^{x^2-y^2}$  and  $Q^{xy}$ , in the fashion of the d-orbitals,  $d^{x^2-y^2}$  and  $d^{xy}$ , as they transform in the same way. Fig. 2 introduces our schematic illustration of the in-plane nematic operators,  $Q^{x^2-y^2}$  and  $Q^{xy}$ , and their linear combinations as appear in the intra-dimer interactions, together with the directions of the  $\mathbf{n}$  vectors.

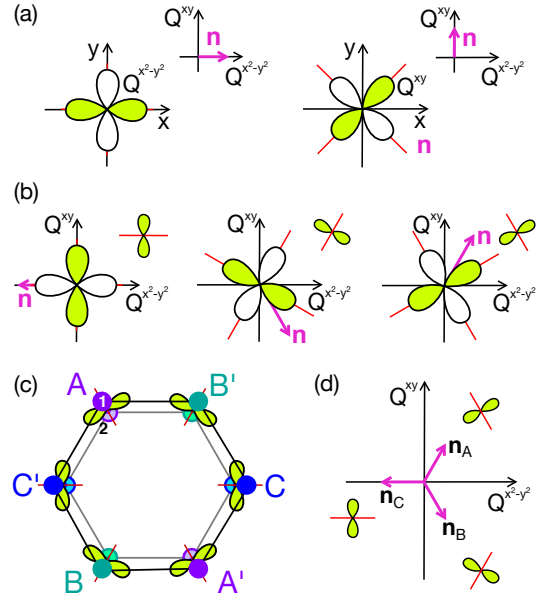


Figure 2: (a) Illustration of the components,  $Q^{x^2-y^2}$  and  $Q^{xy}$ , of the intra-dimer nematic interactions. The pink arrows indicate the direction in the 2-dimensional vector-spaces,  $\mathbf{Q}^{\parallel} = (Q^{x^2-y^2}, Q^{xy})$ . (b) The linear combinations appearing in the intra-dimer in-plane nematic terms. We plot the vectors  $\mathbf{n}$  and the schematic representation of the operators in the same figure. The sketches in the top right corner show the simplified illustration for a given linear combination. (c) Intra-dimer nematic operators on the bonds, and (d) the vectors  $\mathbf{n}_A$ ,  $\mathbf{n}_B$ , and  $\mathbf{n}_C$ , corresponding to the linear combination on each dimer.

Due to the bond-inversion, the antisymmetric exchange anisotropy, i.e. the Dzyaloshinskii–Moriya interaction is not allowed on the dimers.

## B. First neighbor inter-dimer interactions

Classifying the first neighbor inter-dimer interactions, we find six independent operators that transform as the fully symmetric irreducible representation. Beside the anisotropy in the Heisenberg exchange, distinguishing the in-plane and out-of-plane components

$$\mathcal{H}_{\text{XXZ}}^{\text{1st}} = J'_{\parallel} \sum_{\langle i,j \rangle, l=1,2} (S_{i,l}^x S_{j,l}^x + S_{i,l}^y S_{j,l}^y) + J'_{\perp} \sum_{\langle i,j \rangle, l=1,2} S_{i,l}^z S_{j,l}^z, \quad (5)$$

there are additional four operators, namely the in-plane and out-of-plane components of the nematic and DM interactions. The DM interaction has the form

$$\mathcal{H}_{\text{DM}}^{\text{1st}} = \sum_{\langle i,j \rangle} \mathbf{D}' \cdot (\mathbf{S}_i \times \mathbf{S}_j), \quad (6)$$

and the in-plane ( $D'_{\parallel}$ ) and out-of-plane ( $D'_{\perp}$ ) components of the vector  $\mathbf{D}'$  are shown in Fig. 3.

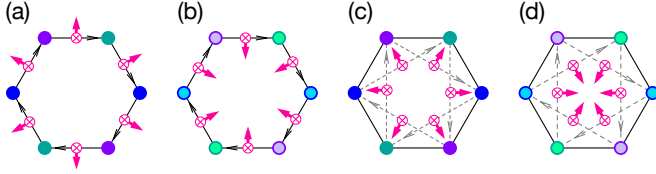


Figure 3: (a-b) DM vector components on the first, and (c-d) on the second neighbor inter-dimer bonds in the top and bottom layers, respectively. For both, the first and second neighbor DM interactions the in-plane components have opposite signs in the top and bottom layer, while the out-of-plane components are the same.

$D'_{\perp}$  is uniform in the top and bottom layers, but the  $D'_{\parallel}$  components change sign under exchanging the layers. As discussed in Section III, only the uniform out-of-plane DM component  $D'_{\perp}$  appears in Bogoliubov–de Gennes Hamiltonian describing the triplet dynamics.

In addition, there are in-plane and out-of-plane bond-nematic terms. The in-plane component has the form of

$$\mathcal{H}_{\parallel}^{\text{1st}} = K'_{\parallel} \sum_{\langle i,j \rangle} \sum_{l=1,2} \mathbf{n}_{ij} \cdot \mathbf{Q}_{il,jl}^{\parallel}, \quad (7)$$

where  $\mathbf{Q}_{il,jl}^{\parallel}$  is defined the same way as 4, the index  $l$  takes the value 1 for the top, and 2 for the bottom layer, while  $i$  and  $j$  denote first neighbor sites within the layers. The vectors  $\mathbf{n}_{ij}$  have the form

$$\mathbf{n}_{A'B} = \mathbf{n}_{AB'} = (-1, 0), \quad (8)$$

$$\mathbf{n}_{B'C} = \mathbf{n}_{BC'} = \left( \frac{1}{2}, \frac{\sqrt{3}}{2} \right), \quad (9)$$

$$\mathbf{n}_{C'A} = \mathbf{n}_{CA'} = \left( \frac{1}{2}, -\frac{\sqrt{3}}{2} \right). \quad (10)$$

The in-plane component of the inter-dimer nematic interactions on the first neighbors are shown in Fig. 4, where we use the same notation introduced in Fig. 2 (a) and (b).

As with the out-of-plane DM components, the in-plane nematic terms are uniform in the top and bottom layers, and so will give a finite contribution to a Hamiltonian for triplets.

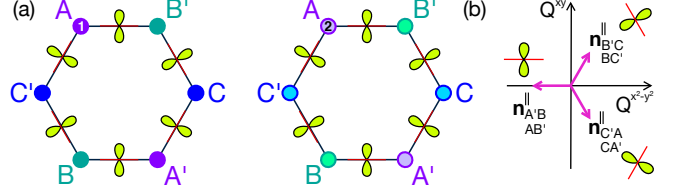


Figure 4: (a) Inter-dimer in-plane symmetric exchange anisotropy  $\mathbf{Q}_{i,j}^{\parallel}$  in the top (left) and bottom (right) layers. (b) Components of the inter-dimer nematic operators between the first neighbor bonds.

The first-neighbor out-of-plane bond-nematic interaction is

$$\mathcal{H}_{\perp}^{\text{1st}} = K'_{\perp} \sum_{\langle i,j \rangle} \mathbf{n}_{ij}^{\perp} \cdot \mathbf{Q}_{il,jl}^{\perp}, \quad (11)$$

where the vectors  $\mathbf{n}_{ij}^{\perp}$  are shown in Fig. 5(b), and the components of  $\mathbf{Q}_{i,j}^{\perp} = (Q_{i,j}^{zx}, Q_{i,j}^{yz})$  correspond to the bond-nematic operators

$$Q_{i,j}^{xz} = S_i^z S_j^x + S_i^x S_j^z, \quad (12a)$$

$$Q_{i,j}^{yz} = S_i^y S_j^z + S_i^z S_j^y. \quad (12b)$$

We utilize the representation of the  $d^{yz}$  and  $d^{zx}$  orbitals, to illustrate the out-of-plane bond-nematic terms as shown in Fig. 5.

Once again, the out-of-plane inter-dimer symmetric exchange anisotropy term is the opposite in the top and bottom layers. For this reason, as with the in-plane DM vectors, it will cancel in the triplet hopping Hamiltonian discussed in Section III.

## C. Second neighbor inter-dimer interactions

We also consider the effect of second-neighbour interactions within the planes of the Kagome lattice. As with the first-neighbor interactions, there are six different terms: XXZ exchange  $J'_{\parallel}$  and  $J'_{\perp}$ ; in-plane and out-of-plane DM interactions,  $D'_{\parallel}$  and  $D'_{\perp}$ ; and the in-plane and out-of-plane bond-nematic terms  $K'_{\parallel}$  and  $K'_{\perp}$ . XXZ interactions are defined through

$$\begin{aligned} \mathcal{H}_{\text{XXZ}}^{\text{2nd}} = & J''_{\parallel} \sum_{\langle\langle i,j \rangle\rangle} \sum_{l=1,2} S_{i,l}^x S_{j,l}^x + S_{i,l}^y S_{j,l}^y \\ & + J''_{\perp} \sum_{\langle\langle i,j \rangle\rangle} \sum_{l=1,2} S_{i,l}^z S_{j,l}^z, \end{aligned} \quad (13)$$

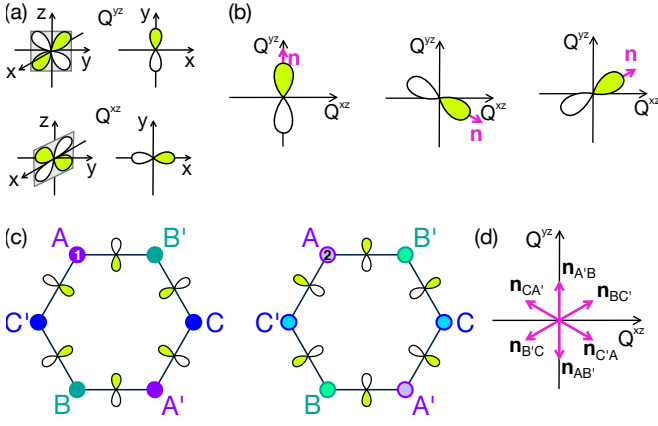


Figure 5: (a) Illustration of the out-of-plane nematic interaction components,  $Q^{zx}$  and  $Q^{yz}$ . The panels on the right show the top-view. (b) Some representative out-of-plane nematic terms and the corresponding  $\mathbf{n}_{ij}^\perp$  vectors (pink arrow), defining the linear combination of  $Q^{zx}$  and  $Q^{yz}$ . (c) Inter-dimer out-of-plane symmetric exchange anisotropy in the top (left) and bottom layer (right). (d) Directions of the first neighbor out-of-plane nematic vectors in the top layer. The directions in the bottom layer are the opposite.

where the sum  $\langle\langle i, j \rangle\rangle$  runs over second-neighbor bonds within the Kagome layers. Similarly, DM interactions are defined through

$$\mathcal{H}_{\text{DM}}^{2\text{nd}} = \sum_{\langle\langle i, j \rangle\rangle} \mathbf{D}'' \cdot (\mathbf{S}_i \times \mathbf{S}_j), \quad (14)$$

where the components of the associated DM vectors in the top and bottom layers are shown in Fig. 3 (d) and (e), respectively.

The additional bond-nematic-type interactions have the form

$$\mathcal{H}_{\parallel}^{2\text{nd}} = K_{\parallel}'' \sum_{\langle\langle i, j \rangle\rangle} \sum_{l=1,2} \mathbf{n}_{ij} \cdot \mathbf{Q}_{il,jl}^{\parallel}, \quad (15)$$

where the vector operator,  $\mathbf{Q}_{il,jl}^{\parallel}$  is defined in 4;  $l$  takes the values 1 and 2 for top and bottom layers, respectively and the vectors  $\mathbf{n}_{ij}$  have the form

$$\mathbf{n}_{AB} = \mathbf{n}_{A'B'} = (1, 0), \quad (16)$$

$$\mathbf{n}_{BC} = \mathbf{n}_{B'C'} = \left(-\frac{1}{2}, -\frac{\sqrt{3}}{2}\right), \quad (17)$$

$$\mathbf{n}_{CA} = \mathbf{n}_{C'A'} = \left(-\frac{1}{2}, \frac{\sqrt{3}}{2}\right). \quad (18)$$

The out-of-plane bond-nematic term is

$$\mathcal{H}_{\perp}^{2\text{nd}} = K_{\perp}'' \sum_{\langle\langle i, j \rangle\rangle} \sum_{l=1,2} \mathbf{n}_{ij}^{\perp} \cdot \mathbf{Q}_{il,jl}^{\perp}, \quad (19)$$

where the components of  $\mathbf{Q}_{i,j}^{\perp} = (Q_{il,jl}^{zx}, Q_{il,jl}^{yz})$  are introduced in Eqs. 12 and the associated vectors  $\mathbf{n}_{ij}^{\perp}$  are shown

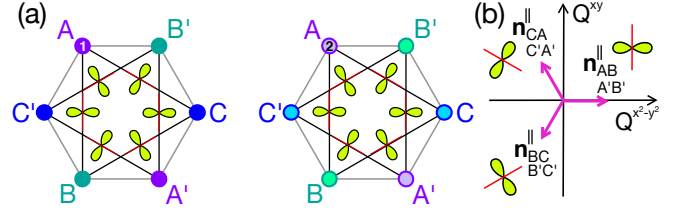


Figure 6: (a) Inter-dimer in-plane symmetric exchange anisotropy  $Q_{i,j}^{\parallel}$  between the second neighbors in the top (left) and bottom (right) layers. (b) Components of the inter-dimer nematic operators.

in Fig. 7(b).

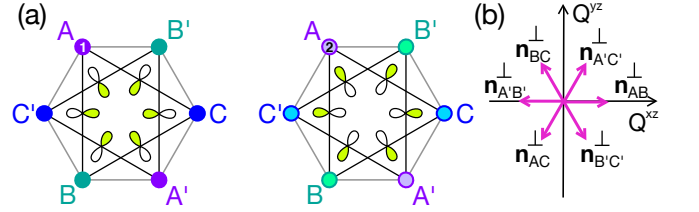


Figure 7: (a) Inter-dimer out-of-plane symmetric exchange anisotropy on the second neighbor bonds in the top (left) and bottom layer (right). We use the notation for the linear combinations of  $Q^{zx}$  and  $Q^{yz}$  bond-nematic operators as shown in Fig. reffig:symmetries. (b) Directions of the second neighbor out-of-plane nematic vectors in the top layer. The directions in the bottom layer are the opposite.

### III. MODEL OF TRIPLON BANDS

Having established the most general form of interactions allowed by symmetry, we now show how this determines the Hamiltonian for triplet excitations of a quantum paramagnet on the bilayer Kagome lattice. We begin by defining the model [Section III A], before proceeding to a Hamiltonian expressed in terms of a bond-wave formalism [Section III B]. Finally, we set up the framework for subsequent discussion of topological bands, by solving for the (topologically-trivial) triplon bands in the limit of vanishing anisotropic exchange [Section III C].

#### A. Microscopic Model

We start from a model defined by

$$\mathcal{H} = \mathcal{H}_{\text{D}_{6h}}^{1,2} + \mathcal{H}_{\text{Zeeman}} \quad (20)$$

$$= \mathcal{H}_{\text{XXZ}} + \mathcal{H}_{\text{DM}} + \mathcal{H}_{\text{Nematic}} + \mathcal{H}_{\text{Zeeman}}, \quad (21)$$

where  $\mathcal{H}_{\text{D}_{6h}}^{1,2}$  [Eq. (1)] is the most general Hamiltonian for a spin-1/2 magnet on a bilayer Kagome lattice with first-

second-neighbour interactions [cf. Section III], and

$$\mathcal{H}_{\text{Zeeman}} = -g_z h^z \sum_i S_i^z, \quad (22)$$

encodes the effect of a magnetic field perpendicular to the plane of the Kagome lattice.

The largest term model in this is taken to be (approximately) Heisenberg exchange  $J_{\parallel} \approx J_{\perp}$  on intra-dimer bonds [Section II A]. Where these interactions are antiferromagnetic, and sufficiently large compared with other terms, the ground state of  $\mathcal{H}_{\text{XXZ}}$  is a quantum paramagnet formed by a product of singlets on all dimer bonds

$$|\Psi_0\rangle = \prod_{j \in \mathbf{1}} |s\rangle_j, \quad (23)$$

where

$$|s\rangle_j = \frac{1}{\sqrt{2}}(|\uparrow_1\downarrow_2\rangle - |\downarrow_1\uparrow_2\rangle)_j. \quad (24)$$

The low-lying excitations of this quantum paramagnet will be spin-1 triplet excitations,

$$|t_1\rangle_j = |\uparrow_1\uparrow_2\rangle_j \quad (25a)$$

$$|t_0\rangle_j = \frac{1}{\sqrt{2}}(|\uparrow_1\downarrow_2\rangle + |\downarrow_1\uparrow_2\rangle)_j \quad (25b)$$

$$|t_{-1}\rangle_j = |\downarrow_1\downarrow_2\rangle_j, \quad (25c)$$

where the indices 1 and 2 denote the dimer-constituting sites in the top and bottom layers, and  $j$  labels the dimer. In the presence of terms connecting different dimers, these triplet excitations will form dispersing bands of excitations, usually referred to as ‘‘triplons’’.

In general, all components of the different exchange interactions within the Kagome planes will contribute to triplon dispersion. For small to moderate spin-orbit coupling, the largest contributions will come from (approximately) Heisenberg interactions on first-neighbour bonds  $J'_{\parallel} \approx J'_{\perp}$ . However the Berry phase underpinning a topological bandstructure originates in DM interactions,  $\mathcal{H}_{\text{DM}}$ . And the fate of these topological bands will in turn depend on the nematic interactions,  $\mathcal{H}_{\text{Nematic}}$ . A few comments are therefore due on how these enter the problem.

Our model allows for DM interactions on first-neighbour bonds,  $\mathbf{D}'$  [Eq. (6)], and second-neighbour bonds,  $\mathbf{D}''$  [Eq. (14)], illustrated in Fig. 3. The inter-layer bond-inversion symmetry precludes any DM interaction acting on the local dimers, and consequently the mixing between the odd singlet and even triplet states. Furthermore, due to the  $\sigma_h$  reflection symmetry, only the uniform out-of-plane DM components,  $\mathbf{D}' = (0, 0, D')$  and  $\mathbf{D}'' = (0, 0, D'')$ , survive in the triplet Hamiltonian to linear order.

Similar considerations apply to nematic interactions  $\mathcal{H}_{\text{Nematic}}$ . In this case, the sign of the out-of-plane nematic terms is opposite in the layers, leaving only the in-plane components in the triplet Hamiltonian.  $\mathcal{H}_{\text{Nematic}}$  thus simplifies to

only the intra-dimer and inter-dimer in-plane nematic interactions, introduced in Eq. (3), Eq. (7), and (15).

Without loss of generality, we consider only the first neighbour interactions. The further neighbor terms do not change the overall shape (and generality) of the triplet Hamiltonian, only add to the complexity of the coefficients. Though, we keep the second neighbour DM interaction ( $D''$ ) to discuss band touching topological transitions as the functions of  $D'$  and  $D''$ .

In the remainder of this paper we will slowly build up a complete picture of the topological physics of a quantum paramagnet described by Eq. (21), starting in Section IV from a simplified model with only Heisenberg and DM interactions, before progressively restoring the complexity of the full Hamiltonian, including nematic terms. Before doing so, in what follows, we set up the necessary technical framework for evaluating triplon bands.

## B. Bond-wave Hamiltonian

To describe the dynamics of the triplet excitations, we rely on the conventional bond wave theory<sup>47,48</sup> resulting in the Bogoliubov-de Gennes Hamiltonian

$$\mathcal{H} = \sum_{\mathbf{k}} \begin{pmatrix} \mathbf{t}_{\mathbf{k}}^{\dagger} \\ \mathbf{t}_{-\mathbf{k}} \end{pmatrix} \begin{pmatrix} M_{\mathbf{k}} & N_{\mathbf{k}} \\ N_{-\mathbf{k}}^{\dagger} & M_{-\mathbf{k}}^{\dagger} \end{pmatrix} \begin{pmatrix} \mathbf{t}_{\mathbf{k}} \\ \mathbf{t}_{-\mathbf{k}}^{\dagger} \end{pmatrix}, \quad (26)$$

where the vector  $\mathbf{t}_{\mathbf{k}}^{\dagger}$  contains the 9 different triplets excitations, corresponding to the three spin states and 3 sublattices;  $(t_{A_{1,\mathbf{k}}}, t_{B_{1,\mathbf{k}}}, t_{C_{1,\mathbf{k}}}, t_{A_{0,\mathbf{k}}}, t_{B_{0,\mathbf{k}}}, t_{C_{0,\mathbf{k}}}, t_{A_{-1,\mathbf{k}}}, t_{B_{-1,\mathbf{k}}}, t_{C_{-1,\mathbf{k}}})$ ,  $\mathbf{k}$  is the momentum and  $M_{\mathbf{k}}$  and  $N_{\mathbf{k}}$  are 9-by-9 matrices, corresponding to the hopping hamiltonian, and the pairing terms, respectively.

The interactions mixing the  $|t_0\rangle$  triplet with the spinful  $|t_1\rangle$  and  $|t_{-1}\rangle$  triplets, are those containing the  $S_i^x S_j^z$  or  $S_i^y S_j^z$ . Such terms are present in the in-plane DM and in the out-of-plane nematic interactions, resulting in  $t_{0,i}^{(\dagger)} t_{\pm 1,j}^{(\dagger)}$  and  $t_{\pm 1,i}^{(\dagger)} t_{0,j}^{(\dagger)}$  terms. These terms are odd under the  $\sigma_h$  reflection, and therefore cancel in the triplet Hamiltonian. As long as  $\sigma_h$  prevails, the  $|t_0\rangle$  triplet remains decoupled from the time-reversal pair  $|t_1\rangle$  and  $|t_{-1}\rangle$  and the most general form of the Bogoliubov-de Gennes Hamiltonian, describing the triplet dynamics, decomposes into two blocks. Due to the cancellation of the in-plane DM terms in the Hamiltonian, the only spin-mixing terms are the in-plane nematic interactions, which can produce a  $\Delta S^z = \pm 2$  transition between the  $|t_1\rangle$  and  $|t_{-1}\rangle$  triplets.

$$\mathcal{H}_{\mathbf{k}} = \begin{pmatrix} \mathbf{t}_{1,\mathbf{k}}^{\dagger} \\ \mathbf{t}_{1,-\mathbf{k}} \\ \mathbf{t}_{0,\mathbf{k}}^{\dagger} \\ \mathbf{t}_{0,-\mathbf{k}} \end{pmatrix} \begin{pmatrix} M_{1,\mathbf{k}} & N_{1,\mathbf{k}} & \mathbf{0} & \mathbf{0} \\ N_{-1,\mathbf{k}} & M_{-1,\mathbf{k}} & \mathbf{0} & \mathbf{0} \\ \mathbf{0} & \mathbf{0} & M_{0,\mathbf{k}} & N_{0,\mathbf{k}} \\ \mathbf{0} & \mathbf{0} & N_{0,\mathbf{k}} & M_{0,\mathbf{k}} \end{pmatrix} \begin{pmatrix} \mathbf{t}_{1,\mathbf{k}} \\ \mathbf{t}_{1,-\mathbf{k}} \\ \mathbf{t}_{0,\mathbf{k}} \\ \mathbf{t}_{0,-\mathbf{k}} \end{pmatrix}, \quad (27)$$

where the  $M_{\pm 1,\mathbf{k}}$  and  $N_{\pm 1,\mathbf{k}}$  are 6-by-6, and  $M_{0,\mathbf{k}}$ , and  $N_{0,\mathbf{k}}$

are 3-by-3 matrices. The vector  $\mathbf{t}_{0,\mathbf{k}}^\dagger$  is  $(t_{A_0,\mathbf{k}}^\dagger, t_{B_0,\mathbf{k}}^\dagger, t_{C_0,\mathbf{k}}^\dagger)$ , and  $\mathbf{t}_{0,-\mathbf{k}} = (t_{A_{0,-\mathbf{k}}}, t_{B_{0,-\mathbf{k}}}, t_{C_{0,-\mathbf{k}}})$ . Furthermore, the spinful subspace is spanned by

$$\begin{aligned} \mathbf{t}_{1,\mathbf{k}}^\dagger &= (t_{A_{+1,\mathbf{k}}}^\dagger, t_{B_{+1,\mathbf{k}}}^\dagger, t_{C_{+1,\mathbf{k}}}^\dagger, t_{A_{-1,\mathbf{k}}}^\dagger, t_{B_{-1,\mathbf{k}}}^\dagger, t_{C_{-1,\mathbf{k}}}^\dagger), \quad \text{and} \\ \mathbf{t}_{1,-\mathbf{k}} &= (t_{A_{-1,-\mathbf{k}}}, t_{B_{-1,-\mathbf{k}}}, t_{C_{-1,-\mathbf{k}}}, t_{A_{+1,-\mathbf{k}}}, t_{B_{+1,-\mathbf{k}}}, t_{C_{+1,-\mathbf{k}}}). \end{aligned} \quad (28)$$

Using this basis, the diagonal and off-diagonal matrices are self-adjoint  $M_{m,\mathbf{k}}^\dagger = M_{m,\mathbf{k}}$ , and  $N_{m,\mathbf{k}}^\dagger = M_{m,\mathbf{k}}$ . Furthermore, as shown below, they only contain even functions of  $\mathbf{k}$ , and therefore  $M_{m,\mathbf{k}} = M_{m,-\mathbf{k}}$  and  $N_{m,\mathbf{k}} = N_{m,-\mathbf{k}}$ . We use the 8 Gell-Mann matrices as the basis for the  $l = 1$  orbital degrees of freedom, corresponding to the three dimers,  $A$ ,  $B$ , and  $C$  in the unit cell.

$$\begin{aligned} \lambda_1 &= \begin{pmatrix} 0 & 1 & 0 \\ 1 & 0 & 0 \\ 0 & 0 & 0 \end{pmatrix}, \lambda_2 = \begin{pmatrix} 0 & -i & 0 \\ i & 0 & 0 \\ 0 & 0 & 0 \end{pmatrix}, \lambda_3 = \begin{pmatrix} 1 & 0 & 0 \\ 0 & -1 & 0 \\ 0 & 0 & 0 \end{pmatrix}, \\ \lambda_4 &= \begin{pmatrix} 0 & 0 & 1 \\ 0 & 0 & 0 \\ 1 & 0 & 0 \end{pmatrix}, \lambda_5 = \begin{pmatrix} 0 & 0 & i \\ 0 & 0 & 0 \\ -i & 0 & 0 \end{pmatrix}, \lambda_6 = \begin{pmatrix} 0 & 0 & 0 \\ 0 & 0 & 1 \\ 0 & 1 & 0 \end{pmatrix}, \\ \lambda_7 &= \begin{pmatrix} 0 & 0 & 0 \\ 0 & 0 & -i \\ 0 & i & 0 \end{pmatrix}, \lambda_8 = \begin{pmatrix} 1 & 0 & 0 \\ 0 & 1 & 0 \\ 0 & 0 & -2 \end{pmatrix}, \end{aligned} \quad (29)$$

The Gell-Mann matrices, and the 3-by-3 identity matrix,  $I_3$  sufficiently characterize the spinless  $S^z = 0$  subspace. The hopping Hamiltonian has the form

$$\begin{aligned} M_{0,\mathbf{k}} = M_{0,\mathbf{k}}^{\text{XXZ}} &= J_{\parallel} \cdot I_3 + J_{\perp} \left[ \cos \frac{\delta_1 \mathbf{k}}{2} \cdot \lambda_4 \right. \\ &\quad \left. + \cos \frac{\delta_2 \mathbf{k}}{2} \cdot \lambda_1 + \cos \frac{\delta_3 \mathbf{k}}{2} \cdot \lambda_6 \right] \end{aligned} \quad (30)$$

and the pairing terms are the same as  $M_{0,\mathbf{k}}$  without the diagonal elements.

$$N_{0,\mathbf{k}} = M_{0,\mathbf{k}} - J_{\parallel} \cdot I_3. \quad (31)$$

Note that the Hamiltonian describing the  $S^z = 0$  subspace contains only the Heisenberg terms, the symmetric nematic exchange and the antisymmetric DM interaction does not affect the  $|t_0\rangle$  triplet.

The triplet hopping of the spinful subspace,

$$M_{\pm 1,\mathbf{k}} = M_{\pm 1,\mathbf{k}}^{\text{XXZ}} + M_{\pm 1,\mathbf{k}}^{\text{DM}} + M_{\pm 1,\mathbf{k}}^{\text{Nematic}} \pm M_{\pm 1,\mathbf{k}}^{\text{Zeeman}} \quad (32)$$

in Eq. (27) is a  $6 \times 6$  matrix. Note that  $M_{1,\mathbf{k}}$  only differs from the  $M_{-1,\mathbf{k}}$  in the sign of the Zeeman term. The spin degree of freedom provided by the  $S^z = \pm 1$  triplets is represented by the Pauli matrices  $s^x$ ,  $s^y$ , and  $s^z$ . The 6-dimensional local Hilbert space for the spinful triplets is constructed as the tensor product of the 2-by-2 matrices  $\{I_2, s^x, s^y, s^z\}$  acting on the spin-space, and the 3-by-3 Gell-Mann matrices extended with the identity  $I_3$ , acting in the orbital space. We discuss the various contributions separately. The Heisenberg interaction

only contains the identity operator,  $I_2$  in the spin-space, i.e. it does not affect the spin degrees of freedom, and is the same for the  $|t_1\rangle$  and  $|t_{-1}\rangle$  triplets.

$$\begin{aligned} M_{\pm 1,\mathbf{k}}^{\text{XXZ}} &= \frac{J_{\parallel} + J_{\perp}}{2} \cdot I_2 \otimes I_3 + J_{\parallel} \cos \frac{\delta_1 \mathbf{k}}{2} \cdot I_2 \otimes \lambda_4 \\ &\quad + J_{\parallel} \cos \frac{\delta_2 \mathbf{k}}{2} \cdot I_2 \otimes \lambda_1 + J_{\parallel} \cos \frac{\delta_3 \mathbf{k}}{2} \cdot I_2 \otimes \lambda_6 \end{aligned} \quad (33)$$

The pairing terms from the Heisenberg interaction are similar to  $M_{1,\mathbf{k}}^{\text{Heis}}$ , but have opposite sign and no diagonal elements

$$N_{\pm 1,\mathbf{k}}^{\text{XXZ}} = -M_{\pm 1,\mathbf{k}}^{\text{XXZ}} + \frac{J_{\parallel} + J_{\perp}}{2} \cdot I_2 \otimes I_3. \quad (34)$$

The DM interaction has the form

$$\begin{aligned} M_{\pm 1,\mathbf{k}}^{\text{DM}} &= \left[ D' \cos \frac{\delta_1 \mathbf{k}}{2} + D'' \cos \frac{(\delta_2 - \delta_3) \mathbf{k}}{2} \right] s^z \otimes \lambda_5 \\ &\quad + \left[ D' \cos \frac{\delta_2 \mathbf{k}}{2} + D'' \cos \frac{(\delta_3 - \delta_1) \mathbf{k}}{2} \right] s^z \otimes \lambda_2 \\ &\quad + \left[ D' \cos \frac{\delta_3 \mathbf{k}}{2} + D'' \cos \frac{(\delta_1 - \delta_2) \mathbf{k}}{2} \right] s^z \otimes \lambda_7 \end{aligned} \quad (35)$$

The only operator acting in the spin-space is  $s^z$ , leaving the spin degrees of freedom unchanged, and introducing a sign difference for the DM interaction in the up and down-spin sector.

Let us make some comments on the time-reversal (TR) properties of the Gell-Mann matrices and the pseudo-spin-half operators. The Gell-Mann matrices act in the orbital space, i.e. account for changing the dimer indices,  $A$ ,  $B$ , and  $C$ . Time-reversal symmetry leaves such indices invariant, therefore the real Gell-Mann matrices are TR invariant. As TR symmetry contains a complex conjugation, the imaginary Gell-Matrices are TR breaking, changing sign under TR. A complete analysis on the TR symmetry of the pseudo-spin-half operators is provided in the Appendix A, where we show that while the  $s^z$  is TR-breaking, as one would expect from a spin-operator, the  $s^x$  and  $s^y$  components are TR invariant operators. This is a consequential difference with respect to the original Kane and Mele model, where the Pauli matrices describe a real spin-half Kramers doublet and thus all break TR symmetry.

Coming back to the DM terms in our triplet hopping Hamiltonian in Eq. (35), the appearing cross-product operators are all TR invariant, as both the  $s^z$  spin operator, and the  $\lambda_5$ ,  $\lambda_2$ , and  $\lambda_7$  complex Gell-Mann matrices break the TR symmetry.

The intra-dimer DM interaction is forbidden by the bond-inversion of the dimers, thus there are no diagonal elements in  $M_{1,\mathbf{k}}^{\text{DM}}$  and the form of the pairing terms simply correspond to

$$N_{\pm 1,\mathbf{k}}^{\text{DM}} = -M_{\pm 1,\mathbf{k}}^{\text{DM}} \quad (36)$$

The nematic interactions couple the subspaces of the  $|t_{\pm 1}\rangle$

and  $|t_{-1}\rangle$  triplets. They have the form

$$\begin{aligned} M_{\pm 1, \mathbf{k}}^{\text{Nematic}} &= \frac{K_{\parallel}}{4} \left[ s^x \otimes \lambda_8 - \sqrt{3} s^y \otimes \lambda_3 \right] \\ &+ K'_{\parallel} \cos \frac{\delta_3 \mathbf{k}}{2} \left( -\frac{1}{2} s^x - \frac{\sqrt{3}}{2} s^y \right) \otimes \lambda_6 \\ &+ K'_{\parallel} \cos \frac{\delta_1 \mathbf{k}}{2} \left( -\frac{1}{2} s^x + \frac{\sqrt{3}}{2} s^y \right) \otimes \lambda_4 \\ &+ K'_{\parallel} \cos \frac{\delta_2 \mathbf{k}}{2} \cdot s^x \otimes \lambda_1, \end{aligned} \quad (37)$$

The Gell-Mann matrices in the nematic interaction are the real ones, preserving TR symmetry. The nematic interactions exclusively consist of spin-mixing operators,  $s^x$  and  $s^y$  that are TR invariant terms themselves. (For details see App. A). When the nematic terms are present,  $S^z$  ceases to be a good quantum number, and the spin up and down components mix. Such spin-mixing term is present in the Kane and Mele model too, in the form of a Rashba spin-orbit coupling, enabled by the breaking the mirror-symmetry  $\sigma_h$ . Here, the spin-mixing nematic terms are allowed without breaking  $\sigma_h$ . The TR symmetry does not protect the degeneracy of the spin-up and down triplets at the TR-invariant points in the momentum space, as it would for the Kramers pair electron-spins. Therefore, the nematic term hybridizes the spins, ending the fragile  $Z_2$  topology of the bands, discussed in Sec. VII.

The nematic interaction is allowed on the dimers too. Note that the operators  $\lambda_8$  and  $\lambda_3$  are diagonal in the orbital space, leaving the sublattices unchanged. The  $s^x$  and  $s^y$  operators, however mix the spins, placing the intra-dimer nematic interaction  $K_{\parallel}$  in the diagonal of the block connecting the +1 and -1 triplets. The  $N_{1, \mathbf{k}}^{\text{Nematic}}$  matrix of the pairing terms corresponds again to the  $-M_{1, \mathbf{k}}^{\text{Nematic}}$  minus the ‘diagonal’ elements

$$N_{\pm 1, \mathbf{k}}^{\text{Nematic}} = -M_{\pm 1, \mathbf{k}}^{\text{Nematic}} + \frac{K_{\parallel}}{4} \left[ s^x \otimes \lambda_8 - \sqrt{3} s^y \otimes \lambda_3 \right] \quad (38)$$

Lastly, the out-of plane magnetic field appears in the diagonal of the Hamiltonian as

$$M_{\pm 1, \mathbf{k}}^{\text{Zeeman}} = \mp g_z h_z s^z \otimes I_3 \quad (39)$$

### C. Bond-wave dispersions in the absence of anisotropies

Let us start with the time reversal symmetric case, when the magnetic field is zero. In the isotropic Heisenberg limit,  $J_{\perp} = J_{\parallel} = J$ , and  $J'_{\perp} = J'_{\parallel} = J'$ ,  $D' = 0$ ,  $D'' = 0$ ,  $K_{\parallel} = 0$ , and  $K'_{\parallel} = 0$  the model has SU(2) symmetry, and the Hamiltonian is identical for the three triplets,  $M_{m, \mathbf{k}} = M_{\mathbf{k}}^{\text{SU}(2)}$ , where

$$M_{\mathbf{k}}^{\text{SU}(2)} = J \cdot I_3 + J' \left[ \cos \frac{\delta_1 \mathbf{k}}{2} \cdot \lambda_4 + \cos \frac{\delta_2 \mathbf{k}}{2} \cdot \lambda_1 + \cos \frac{\delta_3 \mathbf{k}}{2} \cdot \lambda_6 \right], \quad (40)$$

for all  $m = 1, 0, -1$ . In this case, each the three bands, coming from the  $l = 1$  orbital flavor, are all threefold degenerate, as the  $m = 1, 0, -1$  have the same energies in the entire Brillouin zone. The dispersion computed from the SU(2) symmetric Bogoliubov–de Gennes Hamiltonian has the form

$$\omega_{1, m} = \sqrt{J(J - 2J')} \quad (41a)$$

$$\omega_{2, m} = \sqrt{J(J + J') - \tilde{J}(\mathbf{k})} \quad (41b)$$

$$\omega_{3, m} = \sqrt{J(J + J') + \tilde{J}(\mathbf{k})}. \quad (41c)$$

with  $\tilde{J}(\mathbf{k}) = J \cdot J' \sqrt{(3 + 2 \sum_{\alpha} \cos \delta_{\alpha} \cdot \mathbf{k})}$ . The threefold spin-degeneracy of these bands is the consequence of the continuous spin-rotation symmetry, rendering the triplet hopping Hamiltonian,  $M_{\mathbf{k}}^{\text{SU}(2)}$   $m$ -independent. Additionally, discrete lattice symmetries give rise to degeneracies between the orbital bands in the form of a linear band touching at the  $K$  and  $K'$  points, and a quadratic band touching at the zone center,  $\Gamma$ .

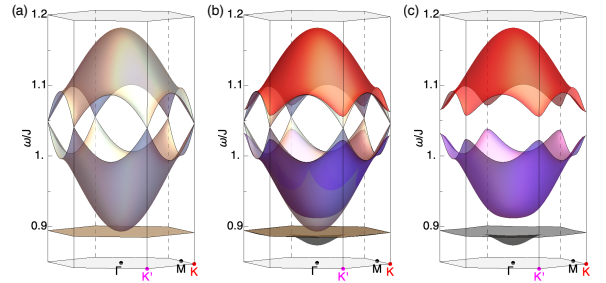


Figure 8: (a) Triplet bands in the SU(2) symmetric case,  $J = 1$ ,  $J' = 0.2$ ,  $h = 0$ , and the DM and nematic terms are zero. All three bands are 3-fold degenerate due to the spin-rotation symmetry. (b) Triplet band structure for finite second neighbor DM interaction,  $D' = 0.01$ . (c) The  $m = \pm 1$  bands omitting the trivial  $m = 0$ . All three bands are twofold degenerate, as a consequence of  $S^z$  being a good quantum number.

In Fig. 8 we show the three, threefold–degenerate bands of this SU(2) symmetric case. The intra-dimer Heisenberg coupling term,  $J$ , is nothing but the singlet–triplet gap, separating the triplet bands from the ground state, while the inter-dimer Heisenberg interaction,  $J'$  gives dispersion to the triplets. The form of dispersion is immediately familiar from studies of graphene<sup>6,7</sup>, with the additional feature of a flat band just above the singlet–triplet gap, reflecting the frustration of the Kagome lattice.

From the band dispersion, Eq. (41), we can also read off the instabilities of the quantum paramagnet. For the ferromagnetic  $J' = -J/4$ , the  $\omega_{3, m}$  softens at the  $\Gamma$  point, signaling a transition to a long-range ordered time-reversal symmetry breaking state, where the spins on each layer are aligned ferromagnetically, while the two layers are aligned antiferromagnetically. Similarly, we may notice that the energy of the  $\omega_{1, m}$  flat band becomes 0 for antiferromagnetic  $J' = J/2$ , indicating a transition to a time-reversal symmetry breaking state, where the ordering is selected by the DM interactions or quantum fluctuations.

#### IV. DM INTERACTION INDUCED BAND TOPOLOGY

In this Section, we explore the effect of the DM interactions on the triplon excitations of a quantum paramagnet described by Eq. (21), keeping the nematic terms and the magnetic field zero. For simplicity, we will also set  $J_{\parallel} = J_{\perp} = J$  in XXZ terms, such that they reduce to isotropic Heisenberg interactions. The analysis is further simplified by the fact that only the  $z$  component of the DM interaction survives (up to first order). It follows that  $S^z$  remains a good quantum number, and excitations with different  $m = 1, 0, -1$  decouple from one another.

The out-of-plane DM interaction lowers the SU(2) symmetry to U(1), and splits the degeneracy at the corners and center of the BZ for the  $m = \pm 1$  triplets. While  $J'$  provides a real hopping amplitude, the inter-dimer DM interactions,  $D'$  and  $D''$  couple to the complex Gell-Mann matrices, and are responsible for the non-trivial topology, generating finite Berry curvature via the complex triplet hopping amplitude. The  $m$ -independent Heisenberg Hamiltonian (40) is extended with the DM interaction (35). As the DM is diagonal with respect to the spin degrees of freedom, we can write the U(1)-symmetric Hamiltonian in a block-diagonal form, with decoupled  $m = 1, 0, -1$  subspaces. We account for the  $s^z$  operator in the DM interaction (35) with the  $m$  factor:

$$\begin{aligned} M_{m,\mathbf{k}}^{U(1)} &= M_{\mathbf{k}}^{\text{SU}(2)} + m \left[ D' \cos \frac{\delta_1 \mathbf{k}}{2} + D'' \cos \frac{(\delta_2 - \delta_3) \mathbf{k}}{2} \right] \lambda_5 \\ &+ m \left[ D' \cos \frac{\delta_2 \mathbf{k}}{2} + D'' \cos \frac{(\delta_3 - \delta_1) \mathbf{k}}{2} \right] \lambda_2 \\ &+ m \left[ D' \cos \frac{\delta_3 \mathbf{k}}{2} + D'' \cos \frac{(\delta_1 - \delta_2) \mathbf{k}}{2} \right] \lambda_7 \end{aligned} \quad (42)$$

To determine the DM gap, we compute the energies at the  $\Gamma$ ,  $K$ , and  $K'$  points. Note that we use the complete Bogoliubov-de Gennes equations, including the pair creation and annihilation terms.

At the  $\Gamma$  point the bands have the energies

$$\omega_{1,m}(\Gamma) = \sqrt{J(J - 2J' - m\Delta_{\Gamma})}, \quad (43a)$$

$$\omega_{2,m}(\Gamma) = \sqrt{J(J - 2J' + m\Delta_{\Gamma})}, \quad (43b)$$

$$\omega_{3,m}(\Gamma) = \sqrt{J(J + 4J')}, \quad (43c)$$

where  $\Delta_{\Gamma} = 2\sqrt{3}(D' + D'')$ . A finite  $\Delta_{\Gamma}$  opens a gap  $\sqrt{J(J - 2J' + \Delta_{\Gamma})} - \sqrt{J(J - 2J' - \Delta_{\Gamma})}$  between the bands 1 and 2 at the  $\Gamma$  point. For  $\Delta_{\Gamma} \ll J, J'$ , the gap becomes  $\approx \sqrt{J/(J - 2J')}\Delta_{\Gamma}$ , thus proportional to the DM interactions.

At the  $K$  and  $K'$  points the bands have energies

$$\omega_{1,m}(K) = \sqrt{J(J - 2J')}, \quad (44a)$$

$$\omega_{2,m}(K) = \sqrt{J(J + J' + m\Delta_K)}, \quad (44b)$$

$$\omega_{3,m}(K) = \sqrt{J(J + J' - m\Delta_K)}, \quad (44c)$$

where  $\Delta_K = \sqrt{3}J(D' - 2D'')$ . This results in a gap of

$\sqrt{J(J + J' + \Delta_K)} - \sqrt{J(J + J' - \Delta_K)}$  at the  $K$  (and  $K'$ ) point between the top bands with nonzero  $m$ . Note that the  $m = 0$  triplet band is not affected by the DM interaction, retaining their degeneracies at  $K$ ,  $K'$ , and  $\Gamma$  points. Furthermore, the  $m = \pm 1$  triplets experience an opposite effect, reflecting the action of the spin-orbit coupling on the up and down spins, lending them an opposite torque. The three

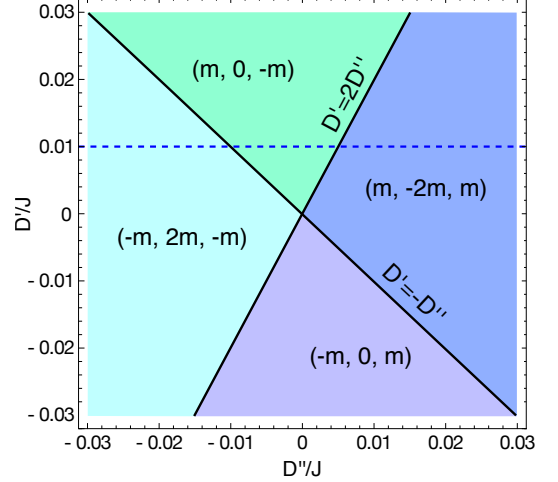


Figure 9: Chern numbers as the function of first ( $D'$ ) and second ( $D''$ ) neighbor inter-dimer DM interaction, listed in order of ascending band energy for a given  $m$ -subspace. The lines  $D' = 2D''$  and  $D' = -D''$  denote the boundaries of the band touching topological transitions. For  $D' = 2D''$  the gap between the upper two bands closes at the corners in the form of Dirac cones. Crossing the  $D' = -D''$  line, the lower bands go through a quadratic touching at the  $\Gamma$  point.

triplet bands within the  $m = 1$  (or  $m = -1$ ) subspace become fully gapped. Although the bands of  $m = 1$  are overlapping with the bands of  $m = -1$  everywhere in the BZ, there are no matrix elements between the two, and the Chern numbers can be computed independently for them<sup>5,49-51</sup>. The triplet bands in the case of a finite DM interaction are plotted in Fig. 8(b) and (c).

To map out a *band touching phase diagram*, we compute the Chern numbers as the function of the first and second neighbor DM interactions,  $D'$  and  $D''$  in Fig. 9. The numbers in Fig. 9 represent the Chern numbers in the  $m$  subspace, going from the bottom band to the top band. The  $m = 1$  and  $m = -1$  triplet bands have opposite Chern numbers, reflecting their opposite chirality.

As the Chern number can only be changed via closing the gap, we can analytically determine the phase boundaries by examining when  $\Delta_{\Gamma}$  or  $\Delta_K$  become zero.

When  $D' = 2D''$ , the  $\Delta_K$  is zero closing the gap between the upper two bands at the  $K$  and  $K'$  points in a linear Dirac-cone-like touching. At each corner points, the Chern number of the bands is changed locally by one as the gap closes and reopens. The contribution from  $K$  and  $K'$  adds up to a  $+2$  and  $-2$  change in the Chern numbers of the upper and middle bands (see Fig. 9). The lowest band remains unaltered.

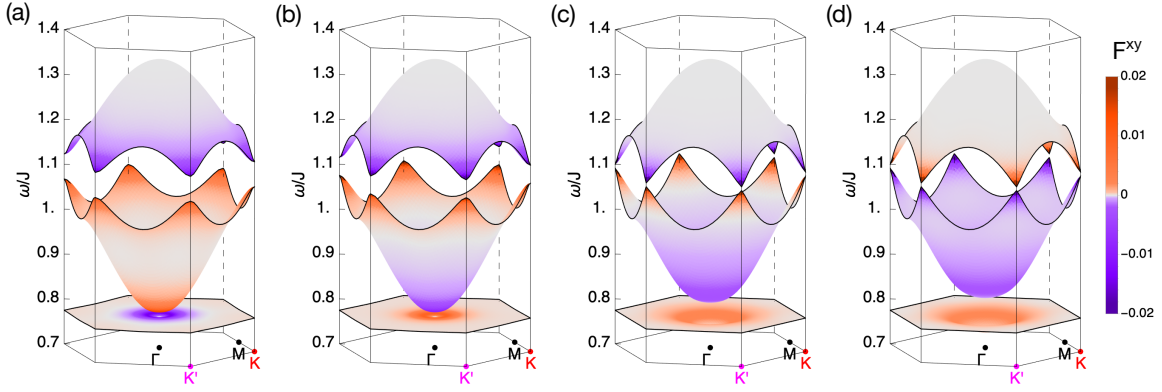


Figure 10: Distribution of Berry curvature in the vicinity of the transition points for the  $m = 1$  bands. The Berry curvature distribution for  $m = -1$  is reversed, and not well defined for  $m = 0$ . At  $D' = -D''$  the gap closes at the  $\Gamma$  point between the middle and lower bands. We chose the values  $J = 1$ ,  $J' = 0.2$ ,  $D' = 0.01$  (a)  $D'' = -0.01 - \epsilon$  and (b)  $D'' = -0.01 + \epsilon$ , where  $\epsilon = 0.0025$ . At  $D' = 2D''$  the gap at  $K$  and  $K'$  closes. Berry curvature for  $D'' = 0.005 - \epsilon$  (c) and  $D'' = 0.005 + \epsilon$  (d).

$\Delta_\Gamma$  becomes zero for  $D' = -D''$  closing the gap between the lower two bands in a quadratic touching at the zone center. The Chern numbers of the lower and middle bands change by  $\pm 2$ . The topmost band is unaffected.

To illustrate the exchange of topological charge across the band touching transitions, we plotted the Berry curvature distribution on the  $m = 1$  triplet bands in the vicinity of  $D' = -D''$  and  $D' = 2D''$  in Fig. 10. The Berry curvature has opposite sign for the  $m = -1$  triplet bands.

When computing the Chern numbers shown in Fig. 9, and the distribution of the Berry curvature in Fig. 10, we use the numerical method introduced in Ref.<sup>51</sup> equipped with the structure for particle-particle terms present in the Bogoliubov–de Gennes type of Hamiltonians. The numerical computation, however, does not provide us a deeper insight. Therefore, in Sec. V, we give a detailed discussion on the topological transitions and the changing of the Chern numbers at the linear and quadratic touching points, restricting our analysis to the hopping part of the Bogoliubov–de Gennes Hamiltonian. The topological properties of the reduced hopping Hamiltonian and the BdG Hamiltonian are the same, as the  $M$  and  $N$  matrices are similar, i.e. they only differ in their diagonal.

## V. LINEAR VERSUS QUADRATIC BAND TOUCHINGS

The transitions between bands with different Chern indices, shown in the phase diagram Fig. 9, occur where the gap between bands closes. The point where bands then touch, may have a linear or quadratic form. In what follows we give a thorough characterization of these linear and quadratic band touchings. We provide analytic expressions for both the Berry curvature, and the associated Chern numbers, before and after the transitions, where they are well defined<sup>52</sup>. Our main focus will be the way in which topological charge is exchanged between bands. In both cases, two units of Chern number are exchanged. For linear band touching this occurs through the

exchange of a single unit at two different points in the BZ,  $K$  and  $K'$ , while for quadratic band touchings two units are exchanged at the  $\Gamma$  point.

We continue with the  $U(1)$  symmetric model of Eq. (42) including the isotropic Heisenberg interaction and the DM interactions, but keeping the nematic terms zero.

Our approach will be to reduce the description of each touching point to a  $2 \times 2$  matrix describing only those bands which touch

$$M_{\mathbf{k}}^{\text{eff}} = d_0(\mathbf{k})I_2 + \mathbf{d}(\mathbf{k}) \cdot \boldsymbol{\sigma}, \quad (45)$$

where  $\boldsymbol{\sigma}$  is a vector of Pauli matrices, and the linear or quadratic form of the band touching is encoded in the coefficients  $d_0(\mathbf{k})$  and  $\mathbf{d}(\mathbf{k})$ . These coefficients can be expanded about the relevant wave vector, thereby allowing the analytic calculation of the Chern number

$$C = \frac{1}{2\pi} \int_{\text{BZ}} \Omega(k_x, k_y) dk_x dk_y \quad (46)$$

through the associated Berry curvature

$$\Omega(k_x, k_y) = \frac{1}{2} \frac{\mathbf{d} \cdot \left( \frac{\partial \mathbf{d}}{\partial k_x} \times \frac{\partial \mathbf{d}}{\partial k_y} \right)}{(\mathbf{d} \cdot \mathbf{d})^{3/2}}, \quad (47)$$

which, in this case, has the interpretation of a Skyrmion density.

For simplicity, the derivation we present is restricted to the hopping matrix  $M_{m,\mathbf{k}}^{U(1)}$ , and neglects the effect of the pair creation and annihilation terms. This restriction can however be relaxed, at the expense of more lengthy expressions. If we were to consider the full Hamiltonian, the unitary transformations would correspond to  $\sigma_z \otimes U_\Lambda$ , ( $\Lambda = K, K', \Gamma$ ), and instead of the  $2 \times 2$  matrix describing the bands in question, we would get a  $4 \times 4$  problem that can be solved using the Bogoliubov transformation. The topological properties of the bands are generally not affected by the pairing terms (an

exception is provided in Ref.<sup>26</sup>, where the diagonal ( $M$ ) and off-diagonal ( $N$ ) matrices were not similar). The equivalency of the topology of  $M$  and the full Hamiltonian has been discussed in Ref. [53].

Ultimately, our goal is to project the three-level problem (of each  $m$ ) onto a two-level one, involving the bands that touch at the corners and the center of the hexagonal Brillouin zone. To do this, we introduce unitary transformations,  $U_K$  and  $U_\Gamma$  that diagonalize  $M_{\mathbf{k}}^{\text{SU}(2)}$  (and  $N_{\mathbf{k}}^{\text{SU}(2)}$  too) at the band touching points. Naturally, we can perform the expansion about the touching point without projecting onto the two levels involved. Nonetheless, we restrict ourselves to a two-level problem to be able to represent the orbital degrees of freedom with only three Pauli matrices instead of eight Gell-Mann matrices, which would give an eight-dimensional  $\mathbf{d}$  vector.

### A. Linear band touching at $K$

We begin with discussing the linear touchings that occur at the corners  $\mathbf{k}_K = (\frac{4\pi}{3}, 0)$  and  $\mathbf{k}_{K'} = (-\frac{4\pi}{3}, 0)$  of the Brillouin

zone for  $D' = 2D''$ . The matrix  $U_K$  that diagonalizes  $M_{\mathbf{k}}^{\text{SU}(2)}$  at both  $K$ -points is

$$U_K = \begin{pmatrix} -\frac{1}{\sqrt{3}} & \frac{1}{\sqrt{2}} & \frac{1}{\sqrt{6}} \\ -\frac{1}{\sqrt{3}} & -\frac{1}{\sqrt{2}} & \frac{1}{\sqrt{6}} \\ \frac{1}{\sqrt{3}} & 0 & \frac{2}{\sqrt{6}} \end{pmatrix}. \quad (48)$$

The column vectors in  $U_K$  correspond to the eigenvectors at  $K$  and also form a basis for the irreducible representations,  $A_1$  and  $E$ , of the three-fold symmetry at these points in the absence of the DM interactions. The band that belongs to the symmetric representation is the bottom band, which is well separated from the upper two bands in the vicinity of the zone-corners. The double representation stretches the subspace that we keep in the linearization. (Let us note that the eigen-energies corresponding to the double representation split for finite DM interaction,  $U_K$  brings  $M_{m,K}^{\text{U}(1)}$  into a block-diagonal form, separating the subspaces, but only diagonalizes the  $M_K^{\text{SU}(2)}$ .) Using  $U_K$ , we transform  $M_{m,\mathbf{k}}^{\text{U}(1)}$  into the form

$$U_K^\dagger \cdot M_{m,\mathbf{k}}^{\text{U}(1)} \cdot U_K = \begin{pmatrix} J - J' & -\frac{1}{4}\sqrt{\frac{3}{2}}J'k_y + im\frac{3}{4\sqrt{2}}D'k_x & \frac{1}{4}\sqrt{\frac{3}{2}}J'k_x + im\frac{3}{4\sqrt{2}}D'k_y \\ -\frac{1}{4}\sqrt{\frac{3}{2}}J'k_y - im\frac{3}{4\sqrt{2}}D'k_x & J + \frac{J'}{2} + \frac{\sqrt{3}}{4}J'k_x & -\frac{\sqrt{3}}{4}J'k_y + im\sqrt{3}\left(\frac{D'}{2} - D''\right) \\ \frac{1}{4}\sqrt{\frac{3}{2}}J'k_x - im\frac{3}{4\sqrt{2}}D'k_y & -\frac{\sqrt{3}}{4}J'k_y - im\sqrt{3}\left(\frac{D'}{2} - D''\right) & J + \frac{J'}{2} - \frac{\sqrt{3}}{4}J'k_x \end{pmatrix}, \quad (49)$$

where  $m$  is the spin-index of the triplets taking the values  $-1, 0, 1$ , and  $k_x$  and  $k_y$  are measured from the  $K$  point, i.e.  $K$  corresponds to  $k_x = k_y = 0$ . At the corners of the Brillouin zone, this matrix is block-diagonal and has eigen-energies  $J - J'$ , and  $J + J'/2 \pm m\sqrt{3}(D'' - D'/2)$ . As we go away from the  $K$  points, small off-diagonal matrix elements appear that are linear in momentum. Projecting (49) on the relevant subspace, we can write the two-band matrix as

$$\mathcal{H}_K^{\text{lin}} = \left(J + \frac{J'}{2}\right) I_2 + \mathbf{d}_K \cdot \boldsymbol{\sigma}. \quad (50)$$

The vector  $\mathbf{d}_K$  has the form

$$d_K^x = -\frac{\sqrt{3}}{4}J'k_y, \quad (51a)$$

$$d_K^y = -m\frac{\sqrt{3}}{2}(D' - 2D''), \quad (51b)$$

$$d_K^z = \frac{\sqrt{3}}{4}J'k_x. \quad (51c)$$

The  $\mathbf{d}_{K'}$  vector for the  $K'$ -point is given by  $(d_{K'}^x, d_{K'}^y, d_{K'}^z) = (-d_K^x, d_K^y, -d_K^z)$ .

Using Eqs. (47) we get

$$\Omega_K(k) = \frac{mJ'^2(D' - 2D'')}{(J'^2k^2 + 4(D' - 2D'')^2)^{3/2}}, \quad (52)$$

where we substituted  $k_x^2 + k_y^2 = k^2$ . We note that the Berry curvature does not depend on the valley index, i.e. it is the same at the  $K$  and  $K'$  points. To obtain a simpler form for  $\Omega(k)$ , we introduce the dimensionless parameter

$$k_0 = \frac{2(D' - 2D'')}{J'}, \quad (53)$$

so that

$$\Omega_K(k) = m\frac{k_0}{2(k^2 + k_0^2)^{3/2}}. \quad (54)$$

$\Omega(k)$  has maximum at  $k = 0$ , i.e. the Berry curvature is concentrated at the  $K$  and  $K'$  points, as shown in Figs. 10 and 11. Then  $\Omega_K = m\frac{\text{sgn}(k_0)}{2k_0^2} \propto m\text{sgn}(D' - 2D'')\frac{J'^2}{(D' - 2D'')^2}$ , which diverges as the  $D' \rightarrow 2D''$ . The  $D' = 2D''$  line marks the band touching transition at the two  $K$ -points as shown in Fig. 9. At this point the  $d_K^y = 0$  and the  $\mathbf{d}_K$  vector is restricted to the  $x$ - $z$  plane. When we go around the  $K$  point in the  $(k_x, k_y)$  plane, the vector  $(d_K^x, d_K^z)$  winds once around the

origin.

Using the definition of the Chern number, Eq. (46), we can integrate the Berry curvature Eq. (54) in a disk around the  $K$  and  $K'$  points that has radius  $k$

$$\begin{aligned} C_K(k) &= \frac{1}{2\pi} \int_0^k \Omega_K(k') 2\pi k' dk' = \\ &= \frac{m}{2} \text{sgn}(k_0) \left( 1 - \frac{|k_0|}{\sqrt{k_0^2 + k^2}} \right). \end{aligned} \quad (55)$$

In the vicinity of the transition point the second term goes to zero, and the  $K$  and  $K'$  points both contribute  $\frac{m}{2}$  to the Chern number. As we cross the transition line  $D' = 2D''$ , i.e. as the  $k_0$  changes sign, the  $\frac{m}{2}$  Berry charge is exchanged and the Chern number is changed by  $\pm 1$  at the  $K$  as well as at  $K'$  – the transferred charge is determined by the winding number at the touching point. The total change of the Chern number, adding up the contribution of  $K$  and  $K'$ , is therefore  $\pm 2$ , as indicated in Fig. 9.

### B. Quadratic band touching at $\Gamma$

The quadratic touching is a little different. In the following, we will show that the total Berry charge is exchanged at a

single point, where the Chern number changes by  $\pm 2$ . Thus, at the quadratic touching the bands have twice as much Berry charge as at the linear touching point. Furthermore, the Berry curvature in the case of the quadratic touching is not centered at a single point, as was the case with the linear touching. Instead, it is concentrate on a ring around the touching point. As the bands approach each other, the radius of the ring decreases, shrinking into a point when the bands touch. To see how this happens, we follow the procedure described above, expanding the rotated  $M_{m,\mathbf{k}}^{U(1)}$  about the  $\Gamma$  point. The transformation matrix that diagonalizes the Heisenberg model  $M_{\mathbf{k}}^{\text{SU}(2)}$  at the zone center has the form

$$U_{\Gamma} = \begin{pmatrix} \frac{1}{\sqrt{3}} & \frac{1}{\sqrt{2}} & \frac{1}{\sqrt{6}} \\ \frac{1}{\sqrt{3}} & -\frac{1}{\sqrt{2}} & \frac{1}{\sqrt{6}} \\ \frac{1}{\sqrt{3}} & 0 & -\frac{2}{\sqrt{6}} \end{pmatrix}. \quad (56)$$

Rotating  $M_{m,\mathbf{k}}^{U(1)}$  with  $U_{\Gamma}$ , it becomes block-diagonal at the  $\Gamma$  point, decoupling the touching bands from the top band. Moving away from the zone center, additional small matrix elements appear between the subspaces,

$$U_{\Gamma}^{\dagger} \cdot M_{\Gamma}^m \cdot U_{\Gamma} = \begin{pmatrix} J - \frac{J'}{8} k^2 + 2J' & -\frac{J'}{8\sqrt{2}} k_x k_y & -\frac{J'}{16\sqrt{2}} (k_x^2 - k_y^2) \\ -\frac{J'}{8\sqrt{2}} k_x k_y & J - J' + \frac{J'}{8} k_x^2 & -im\sqrt{3}(D' + D'') + \frac{J'}{8} k_x k_y \\ -\frac{J'}{16\sqrt{2}} (k_x^2 - k_y^2) & im\sqrt{3}(D' + D'') + \frac{J'}{8} k_x k_y & J - J' + \frac{J'}{8} k_y^2 \end{pmatrix}. \quad (57)$$

where  $k_x^2 + k_y^2 = k^2$ . We keep only the leading terms, taking  $D', D'' \ll J'$  we neglect terms as  $D'k^2$  and  $D''k^2$ . Diagonalizing this matrix at the  $\Gamma$  point we find the energies  $\omega_1 = J + 2J'$  for the upper band, and  $\omega_{2,3} = J - J' \pm m\sqrt{3}(D' + D'')$  for the lower bands split by the DM-interactions [cf. Eq. (43)]. The effective  $2 \times 2$  Hamiltonian describing the splitting in the vicinity of the  $\Gamma$  point is the bottom right corner of the matrix (57),

$$H_{\Gamma}^{\text{eff}} = J - J' \left( 1 - \frac{k^2}{16} \right) I_2 + \mathbf{d}_{\Gamma} \cdot \boldsymbol{\sigma}, \quad (58)$$

where the first term is an energy shift, and the  $\mathbf{d}_{\Gamma}$  reads

$$d_{\Gamma}^x = \frac{1}{16} J' 2k_x k_y, \quad (59a)$$

$$d_{\Gamma}^y = m\sqrt{3}(D' + D''), \quad (59b)$$

$$d_{\Gamma}^z = \frac{1}{16} J' (k_x^2 - k_y^2). \quad (59c)$$

In the absence of the DM interactions  $d_{\Gamma}^z = 0$ , and we can recognize the mark of the quadratic band touching: as we go

around the  $\Gamma$  point in the  $(k_x, k_y)$  plane, the vector  $(d_{\Gamma}^x, d_{\Gamma}^y)$  winds twice around the origin<sup>54</sup>. Turning on the  $D'$  and/or the  $D''$ , a gap  $\tilde{\Delta}_{\Gamma}(\mathbf{k}) = 2\sqrt{\mathbf{d}_{\Gamma} \cdot \mathbf{d}_{\Gamma}}$  opens between the two bands of the size

$$\tilde{\Delta}_{\Gamma}(\mathbf{k}) = \sqrt{12(D' + D'')^2 + \frac{1}{64} J'^2 k^4}, \quad (60)$$

[c.f. Eq. (43)]. Inserting  $\mathbf{d}_{\Gamma}(\mathbf{k})$  into Eq. (47) for the Berry curvature of the lower band, we get

$$\Omega_{\Gamma}(k) = \frac{4m\sqrt{3}(D' + D'') \left( \frac{J'k}{8} \right)^2}{\left[ 12(D' + D'')^2 + \left( \frac{J'k^2}{8} \right)^2 \right]^{3/2}}, \quad (61)$$

while  $\Omega_{\Gamma}(k)$  changes sign for the upper band. It is convenient to rewrite the curvature as

$$\Omega_{\Gamma}(k) = m \frac{2k^2 k_0^2}{(k_0^4 + k^4)^{3/2}} \text{sgn}(D' + D''), \quad (62)$$

where

$$k_0^2 = 16\sqrt{3} \frac{|D' + D''|}{J'}. \quad (63)$$

$\Omega_\Gamma(k)$  has a maximum for  $k = 2^{-1/4}k_0$ , where it diverges as

$$\Omega_\Gamma(2^{-1/4}k_0) \propto \frac{m}{k_0^2} \text{sgn}(D' + D'') \propto m \frac{J'}{D' + D''} \quad (64)$$

for  $D' + D'' \rightarrow 0$ . Furthermore, the  $\Omega_\Gamma(k)$  vanishes for both  $k \ll k_0$  and  $k \gg k_0$ :

$$\Omega_\Gamma(k) = \begin{cases} m \text{sgn}(D' + D'') \frac{2k^2}{k_0^4} + \dots, & \text{if } k \ll k_0; \\ m \text{sgn}(D' + D'') \frac{2k_0^2}{k^4} + \dots, & \text{if } k \gg k_0. \end{cases} \quad (65)$$

The maximum of the Berry curvature forms a ring around the  $\Gamma$  point. The ring is nicely seen for the lowest two bands in Fig. 10. This behavior is unlike the linear band touching, as there the Berry curvature is concentrated at the  $K$ -points which will touch.

Using Eq. (46) and integrating the curvature around the  $\Gamma$  point, we can check that the ring has enough curvature to collect a contribution  $\pm 1$  to the Chern number of the bands:

$$C_\Gamma(k) = m \text{sgn}(D' + D'') \left( 1 - \frac{k_0^2}{\sqrt{k_0^4 + k^4}} \right) \quad (66)$$

$$\approx m \text{sgn}(D' + D'') \left( 1 - \frac{k_0^2}{k^2} \right), \quad \text{if } k \gg k_0. \quad (67)$$

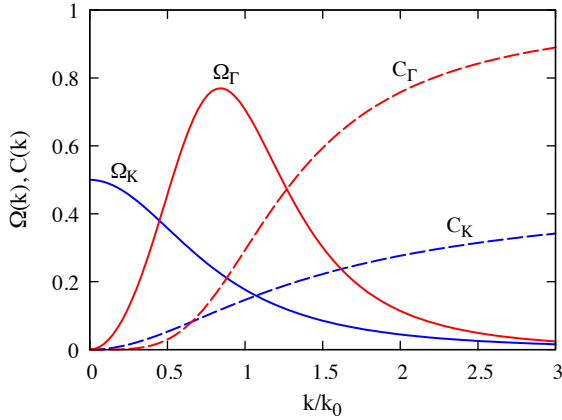


Figure 11: The radial distribution of the Berry curvature  $\Omega(k)$  (solid lines) and the contribution to the Chern number  $C(k)$  (dashed lines) for the linear band touching around the  $K$  points [Eqs. (54) and (55)] and for the quadratic band touching around the  $\Gamma$  point [Eqs. (62) and (66)] in the Brillouin zone. The Berry curvature is maximal at the  $K$  point for linear band touching, while in the case of the quadratic band touching it forms a ring-like structure around the  $\Gamma$  point. In both cases, their integrals over a disk of radius  $k$  centered at the touching points saturates quickly at the 1/2 and 1 values ( $C(k)$ ).

Here  $m = -1, 0, 1$ , and the sign depends on the band as well as the sign of the DM interaction. As the DM is continuously tuned across the the quadratic band touching transition, the  $+1$  and  $-1$  Berry charges are exchanged between the two bands, leading to the  $\Delta C = 2$  transition for the two lowest bands, as seen along the  $D' = -D''$  line in Fig. 9 and 10.

## VI. TRIPLET $Z_2$ TOPOLOGICAL INSULATOR

We now turn to the problem of classifying the topological phases of the model, and characterising their experimental characteristics. We start with the gapped, topological phase found in the simplified model of Section IV, which we show to be a spin-Hall state characterised by a  $Z_2$  topological invariant, in direct analogue with the model of Kane and Mele<sup>7</sup>.

Within each  $m$  subspace, we can think about the DM interaction term as an effective magnetic field in momentum space that acts on a pseudo spin-1 corresponding to the orbital degree of freedom. The  $m = 0$  subspace is clearly no subject to any kind of magnetic field, while the spinful  $m = 1$  and  $-1$  triples are affected in the opposite way. Within the  $m = 1$  and  $-1$  subspace, the effective field (DM) splits the orbital spin-1, making both  $m = 1$ , and  $-1$  a pseudo spin-1 analog to the Haldane model<sup>6</sup>. The time reversal pair  $m = 1$  and  $m = -1$

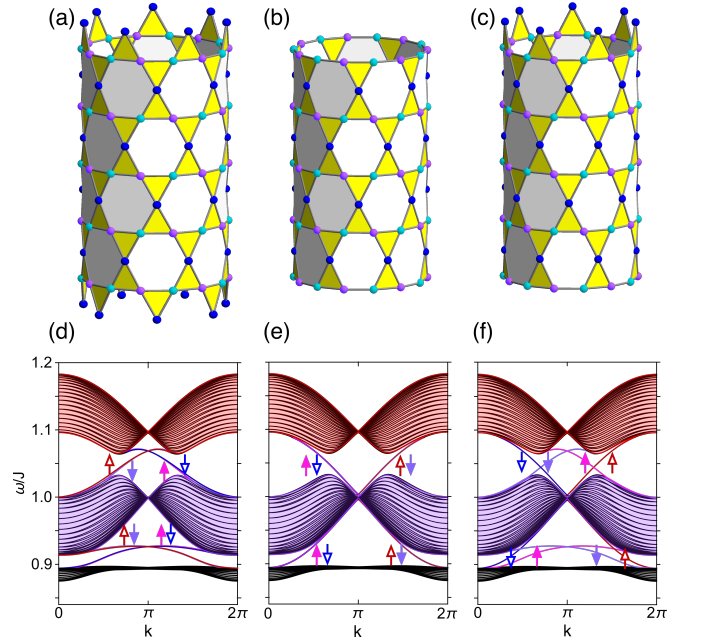


Figure 12: (a)–(c) Schematic figures representing periodic boundaries along the  $x$  direction and a finite size in the  $y$  direction with various edges. (d)–(f) The projected  $m = \pm 1$  triplet bands and helical triplet edge modes for finite second neighbor DM interaction,  $D'' = 0.01$  in the open geometries shown in (a)–(c), respectively. The edge modes are colored according to the spin degrees of freedom and the edges, with red colors representing the up-spin and the blue colors denoting the down-spin. The open arrows correspond to the bottom edge, and the filled ones to the top edge.

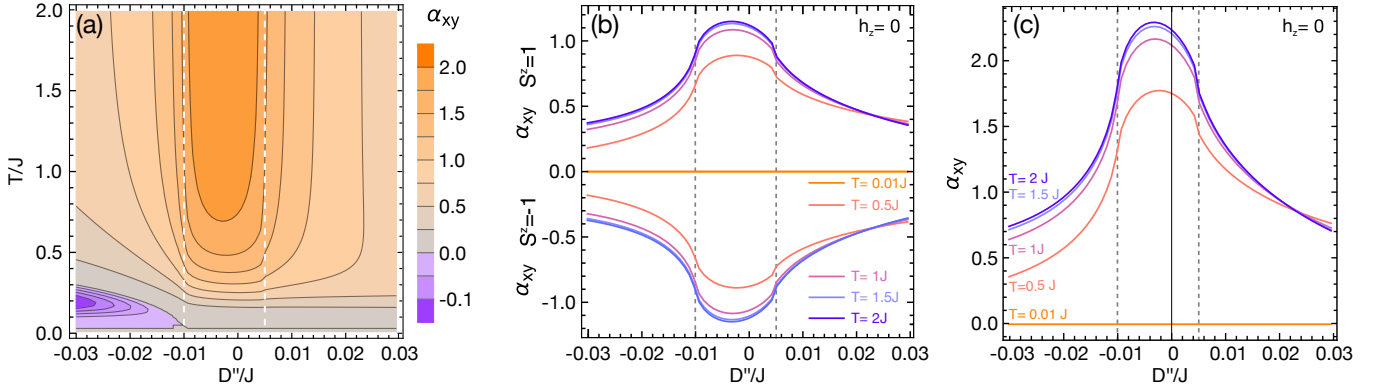


Figure 13: (a) The spin Nernst coefficient,  $\alpha_{xy}$  along the blue dashed line of Fig. 9 as a function of temperature and  $D''$  ( $J'/J = 0.2$ ,  $D'/J = 0.1$ ). The white dashed lines indicate the boundaries of the band touching topological transitions, where the Berry curvatures of the touching bands are exchanged. This change in the topological charge is also signaled by the anomaly of spin Nernst effect at the transition lines. (b) The contributions of the  $S^z = +1$  and  $-1$  triplet bands to the Nernst coefficient as the function of  $D''$  at given temperatures. The  $\alpha_{xy}$  has the same size and an opposite sign for the up and down spins, corresponding to their degenerate energies but opposite chirality. (c) The total  $\alpha_{xy} = \alpha_{1,xy} - \alpha_{-1,xy}$  Nernst coefficient as the function of  $D''$  at various temperature values.

bands realize an analog of the Kane and Mele model. Let us emphasize that the triplets, being components of an integer spin, do not form Kramer's pairs, and their degeneracy may be lifted even when the TR symmetry is preserved. When the nematic exchange anisotropies are present, for example, the  $S^z$  ceases to be a good quantum number, and the  $m = 1$  and  $m = -1$  subspaces hybridize, destroying the  $\mathcal{Z}_2$  phase. We discuss this scenario in Sec. VII

In the case when the nematic terms are zero, the complete overlap between the  $m = 1$  and  $m = -1$  bands renders the net Chern number zero. The  $m = \pm 1$  triplets realize an analog of the spin Hall insulator state and are characterized by a  $\mathcal{Z}_2$  invariant<sup>7–10</sup>.

As shown in Sec. IV, the Chern numbers are multiples of  $m$  (see Fig. 9), and the bands with opposite spin have opposite Chern number. Therefore, the total Chern number of each degenerate band, formed by the time-reversal partners,  $m = \pm 1$ , vanishes:  $C_{n\uparrow} + C_{n\downarrow} = 0$ . Similar to electronic systems with conserved  $S^z$ , the  $\mathcal{Z}_2$  index can be understood as the “spin Chern number”<sup>27</sup> and computed as the staggered quantity  $\frac{1}{2}(C_{n\uparrow} - C_{n\downarrow}) \bmod 2$ .

For the bottom and top bands the Chern numbers in each phase are  $\pm m$ , thus the spin Chern number is  $\pm \frac{2}{2} \bmod 2 = 1$ . The middle band has either Chern number 0, or  $\pm 2m$ , resulting in a trivial 0  $\mathcal{Z}_2$  index. This also shows that the  $\mathcal{Z}_2$  topological invariant does not depend on the DM anisotropy, but only on the conservation of  $S^z$ . Even when we close the band gaps at the band touching transitions, the  $\mathcal{Z}_2$  indices will not change. The  $\mathcal{Z}_2$  index can be computed using the eigenvalues of the parity operator too, which we discuss in detail in the Appendix B.

As a consequence of the  $\mathcal{Z}_2$  topology, the system with open boundaries has helical triplet edge-modes, as shown in Fig. 12. Note that one helical edge state is made of two chiral edge states going in opposite directions. We chose three different edge geometries, illustrated in Fig. 12 (a)–(c), and com-

puted the bands for each of those (see Fig. 12 (d)–(f)). The spin degree of freedom of the edge-modes is denoted with red and blue colors, while the filled and open arrows corresponds to the top and bottom edges, respectively.

### A. Triplet Nernst effect

To obtain an experimentally detectable signature of the  $\mathcal{Z}_2$  triplet bands, we compute the boson analog of the spin Hall effect. Applying a temperature gradient on the sample induces an energy current of triplet excitations. The  $m = 1$  and  $-1$  triplets are affected in an opposite way by the DM interaction, due to their opposite chirality, and deflect into opposite directions. The triplet spin separation perpendicular to the temperature gradient leads to the cancelation of the transverse triplet heat current, but gives a finite transverse spin current. The transverse spin current arising in response to an applied temperature gradient is called the Nernst effect. We directly apply the formula of magnon mediated spin Nernst effect<sup>23,25,36,55,56</sup> for the triplet excitations,  $j_{SN} = \alpha_{xy} \hat{\mathbf{z}} \times \nabla T$ . The spin Nernst coefficient,  $\alpha_{xy}$  can be expressed as

$$\alpha_{xy} = -i \frac{k_B}{\hbar} \sum_{m,n} \int_{\text{BZ}} m \cdot c_1(\rho_{n,m}) F_{n,m}^{xy}(\mathbf{k}) d^2 \mathbf{k}, \quad (68)$$

where  $F_{n,m}^{xy}(\mathbf{k})$  is the Berry curvature of the  $n$ -th band of triplet  $m$ ,

$$c_1(\rho) = \int_0^\rho \ln(1+t^{-1}) dt = (1+\rho) \ln(1+\rho) - \rho \ln \rho \quad (69)$$

and  $\rho_{n,m}$  corresponds to the Bose–Einstein distribution function  $(e^{\omega_{n,m}\beta} - 1)^{-1}$ .

A density plot of the numerically computed triplet mediated spin Nernst coefficient,  $\alpha_{xy}$  is shown in Fig 13 as func-

tion of temperature and  $D''$ . We calculated  $\alpha_{xy}$  along the blue dashed line in Fig. 9, using the complete Bogoliubov–de Gennes Hamiltonian. At the topological band touching lines  $D'' = -D'$  and  $D'' = 2D'$ , the spin Nernst effect has inflection points, corresponding to the exchange of topological charge between the touching bands.

As long as the magnetic field  $h_z$  is zero and the time reversal symmetry is preserved,  $\alpha_{xy,1} = -\alpha_{xy,-1}$ , and the transverse spin Nernst current,  $j_{\text{SN}} = j_{\text{SN},1} - j_{\text{SN},-1}$ , can be written as  $2j_{\text{SN},1}$ . An applied magnetic field Zeeman-splits the triplets, pushing the  $m = 1$  and  $m = -1$  bands in opposite directions (see Sec. VIII). As a consequence, the thermal filling of  $m = 1$  and  $m = -1$  becomes different, leading to an imbalanced contribution from the up and down spins but still providing a finite spin Nernst effect. Note that we consider an out-of-plane field direction, that does not harm the U(1) symmetry, preserving  $S^z$  as good quantum number.

## VII. NEMATIC INTERACTION AND THE FATE OF THE $\mathcal{Z}_2$ PHASE

We now explore the consequences of the terms which mix the triplets with  $m = \pm 1$  — the nematic interactions introduced in Section II. Symmetric exchange anisotropies of this type are naturally present in various spin systems. For example, in single- and bilayer kagome and honeycomb models, routinely proposed to show nontrivial topology.

In the original Kane and Mele model<sup>7</sup>, analogous spin mixing terms, such as the Rashba spin-orbit coupling, can be present (when the  $\sigma_h$  reflection is broken). Although such a term hybridizes the bands with up and down spins, the spin-degeneracy at the time reversal invariant momenta (TRIM) remains, protected by Kramer’s theorem. As a consequence, the  $\mathcal{Z}_2$  topological phase considered by Kane and Mele is *perturbatively* stable against the introduction of Rashba interactions.

To explicitly see the difference for the pseudo-spin-half formed by the  $+1$  and  $-1$  triplets, we compute the energies of the bands at the TRIM. The TRIM, namely  $\Gamma = (0, 0)$ ,  $M_1 = (\pi, \frac{\pi}{\sqrt{3}})$ ,  $M_2 = (0, \frac{2\pi}{\sqrt{3}})$ , and  $M_3 = (-\pi, \frac{\pi}{\sqrt{3}})$  are shown in the bottom panel of Fig. 1(a). Including the nematic terms, the energies at the  $\Gamma$  point become

$$\omega_{1,2}(\Gamma) = J + \frac{J'}{2} - \frac{\sqrt{3}}{2}(D' + D'') - \Lambda, \quad (70a)$$

$$\omega_{3,4}(\Gamma) = J - J' + \sqrt{3}(D' + D'') \pm \frac{1}{2}(K_{\parallel} - 4K'_{\parallel}), \quad (70b)$$

$$\omega_{5,6}(\Gamma) = J + \frac{J'}{2} - \frac{\sqrt{3}}{2}(D' + D'') + \Lambda, \quad (70c)$$

where  $\Lambda = \frac{1}{2}\sqrt{3(D' + D'' + \sqrt{3}J')^2 + (K_{\parallel} + 2K'_{\parallel})^2}$ . At the zone center, the top and bottom bands remain degenerate and the middle two bands split as a result of the nematic interaction.

The effect of the nematic term is more drastic at the less symmetric  $M$  points, where the energies of the six triplets are

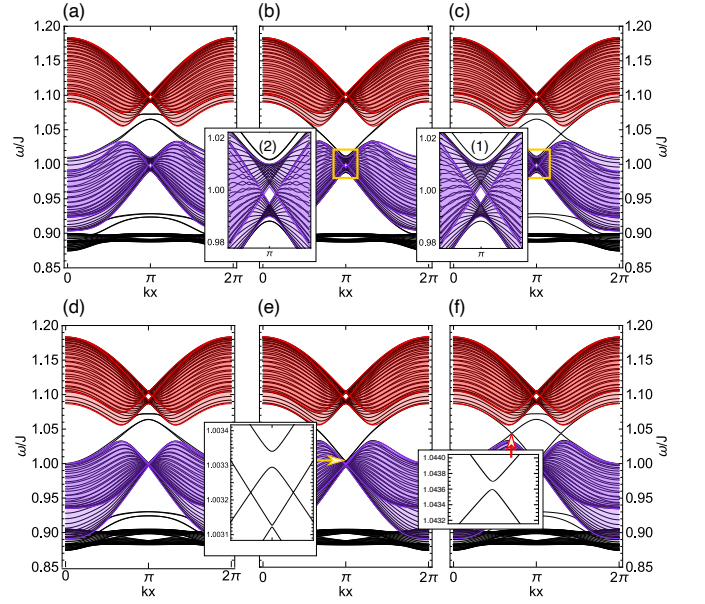


Figure 14: The effect of the nematic interaction on the edge modes and the topology of the bands. (a), (b), and (c) show the case when  $J' = 0.1J$ ,  $D'' = 0.01J$ , and  $K = 0.02J$ , for the spiky, flat, and mixed geometries, respectively (see Fig. 12 (a)–(c)). The finite intra-dimer nematic term leads to the hybridization of the helical edge modes with up and down spin, and a gap is opened at  $k = \pi$  between the boundary-modes on the spiky edges, rendering them topologically trivial. The boundary modes at the flat edges do not merge with the middle band at  $k = \pi$ , but avoid that and become trivial as well as shown in the insets of (b) and (c). (d), (e), and (f) represent the case when the inter-dimer nematic interaction is finite,  $J' = 0.1J$ ,  $D'' = 0.01J$ , and  $K' = 0.01J$ . Here too the edge-modes with up and down spins hybridize and become gapped at  $\pi$ . In the case of the mixed boundaries, the edge-modes merge hybridization within the gap (see inset of (f)), and thus cannot not collapse the band-gap, signaling topologically trivial bands.

all nondegenerate

$$\omega_{1,2}(\Gamma) = J \mp K'_{\parallel} - \Lambda_{\pm}, \quad (71a)$$

$$\omega_{3,4}(\Gamma) = J \mp \frac{K_{\parallel}}{2}, \quad (71b)$$

$$\omega_{5,6}(\Gamma) = J \mp K'_{\parallel} + \Lambda_{\pm}, \quad (71c)$$

with  $\Lambda_{\pm} = \frac{1}{2}\sqrt{(2J' - \frac{K_{\parallel}}{2})^2 + (2(D' - D'') \pm \frac{\sqrt{3}}{2}K_{\parallel})^2}$ . For simplicity, the eigenvalues and band-gaps have been calculated considering the  $M_{\mathbf{k}}$  matrix and not the entire Bogoliubov–de Gennes problem. Solving the BdG problem denies us a simple analytical form, however, the physics remains the same: The nematic terms open a gap at the TRIM, and the spin-degeneracy is not preserved as opposed to the case of the Kramer’s-doublets of the original Kane-Mele model.

To show the effect of the nematic terms on the  $\mathcal{Z}_2$  topology, we compute the bands of the bilayer kagome stripes for the three different edge types shown in Fig. 12 (a)–(c). In an open

system, the time reversal invariant point is  $k = \pi$ . The spin-degeneracy at this point will not necessarily be protected by TR symmetry, as it were for a Kramer's pair. In Fig. 14, we plot the spinful triplet bands for the various edge-geometries for finite intra-dimer nematic interaction (panels (a)–(c)) and for finite inter-dimer nematic interaction (panels (d)–(f)). We find that in each cases the edge modes hybridize, becoming trivial via an avoided crossing, i.e. they no longer connect the bands and close the gap. This is a clear indication that the fragile  $\mathcal{Z}_2$  topology is quashed by the nematic terms.

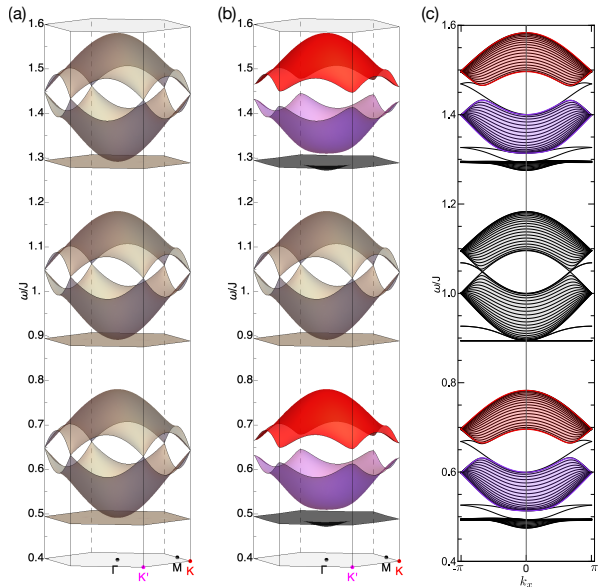


Figure 15: The finite magnetic field ( $h = 0.2J$ ,  $g_z = 2$ ) splits the triplets according to their spin degree of freedom  $m$ . (a) Triplet bands for the  $D' = D'' = 0$  isotropic case. The bands of each  $m$  sector have the same dispersion shifted by the Zeeman energy (b)  $D' = 0$ ,  $D'' = 0.01J$ . The  $m = \pm 1$  bands become fully gapped with well defined and finite Chern numbers, while the  $m = 0$  modes remain unaffected. (c) 1D dispersion in the open geometry (corresponding to Fig. 12(a)) for the  $D' = 0$ ,  $D'' = 0.01J$  case. Nontrivial edge states collapse the anisotropy gaps for  $m = \pm 1$ , signaling nontrivial band topology.

### VIII. TIME-REVERSAL SYMMETRY BREAKING AND THERMAL HALL EFFECT

So far, we have only considered states found in the absence of magnetic field. However the breaking of time-reversal symmetry by magnetic field also has interesting consequences. In Fig. 15, we show how the triplon band structure of a model with Heisenberg and DM interactions changes as a function of magnetic field.

An immediate consequence of magnetic field is that the time-reversal pairs  $m = \pm 1$  split, and their Chern numbers no longer cancel. As a result, we end up with an analog of a Chern insulator state, but realized by the triplets.

A second consequence of the Zeeman splitting of triplets

is that the thermal filling of  $m = 1$  and  $m = -1$  becomes different, and the imbalance of the up and down spin current produces a finite thermal Hall coefficient. The thermal Hall signal is the transverse energy current in response to an applied temperature gradient (and perpendicular magnetic field). In the TR symmetric case the up and down-spin triplets had overlapping energies and consequently identical thermal filling, providing the same number of excitations moving in opposite directions and giving a zero net thermal Hall response. As the degeneracy is lifted, the up and down-spin contributions become different giving a finite net transverse energy current. The thermal Hall coefficient can be written as<sup>38</sup>.

$$\kappa_{xy} = -i \frac{1}{\beta} \sum_{n,m} \int_{\text{BZ}} c_2(\rho_{n,m}) F_{n,m}^{xy}(\mathbf{k}) d^2\mathbf{k}, \quad (72)$$

where  $F_{n,m}^{xy}(\mathbf{k})$  is the Berry's curvature,  $c_2(\rho) = \int_0^\rho \ln^2(1+t^{-1}) dt$ , and  $\rho_{n,m}$  is the Bose-Einstein distribution.

We computed the thermal Hall coefficient,  $\kappa_{xy}$  along the blue dotted line indicated in Fig. 9 as the function of temperature and using the entire Bogoliubov–de Gennes Hamiltonian.  $\kappa_{xy}$  is plotted in Fig. 16.

In summary, the parameters  $D'$  and  $D''$  together with the Chern numbers define a topological phase diagram as seen on Fig. 9. The different phases can be clearly distinguished by the thermal Hall coefficient which is largest in the  $(m, 0, -m)$  phase, as can be seen on Fig. 16. The effect is equally large in the  $(-m, 0, m)$  phase, but of opposite sign, as this phase can be reached simply by inverting the sign of  $D'$  and  $D''$  thereby negating the sign of the  $m$ -dependent term in the Hamiltonian.

### IX. CONCLUSIONS

In this Article, we investigate the topology of the triplon bands found in spin-1/2 quantum paramagnet on bilayer kagome lattice. We go beyond the XXZ model extended with the DM interactions, the archetypal analogue of the electronic tight-binding hopping Hamiltonian with spin-orbit coupling. Deriving the most general form of the Hamiltonian allowed by the symmetry of the lattice [Section II] we explore the ramifications of each symmetry-allowed terms. Reducing the Hamiltonian to a model for triplon excitations of the quantum paramagnet [Section III], we characterize these bands for models of increasing complexity, by lowering the symmetries.

The simplest case is when the Hamiltonian is the pure  $SU(2)$  symmetric Heisenberg model, discussed in Sec. III C. In this case, the band structure is trivial, with 3-fold degenerate bands, exhibiting a quadratic band touching at the  $\Gamma$  point and linear band touchings at the  $K$  and  $K'$  points in the Brillouin zone.

When the DM interactions reduce the symmetry of the model to  $TR \times U(1)$ , we find that the triplets provide an analog to the  $\mathcal{Z}_2$  topological insulator considered by Kane and Mele<sup>7,8</sup>, with helical triplet modes on open edges [Section IV]. This model supports topological phases with bands having different Chern numbers. We give a detailed description of the exchanged topological charges at the phase transitions,

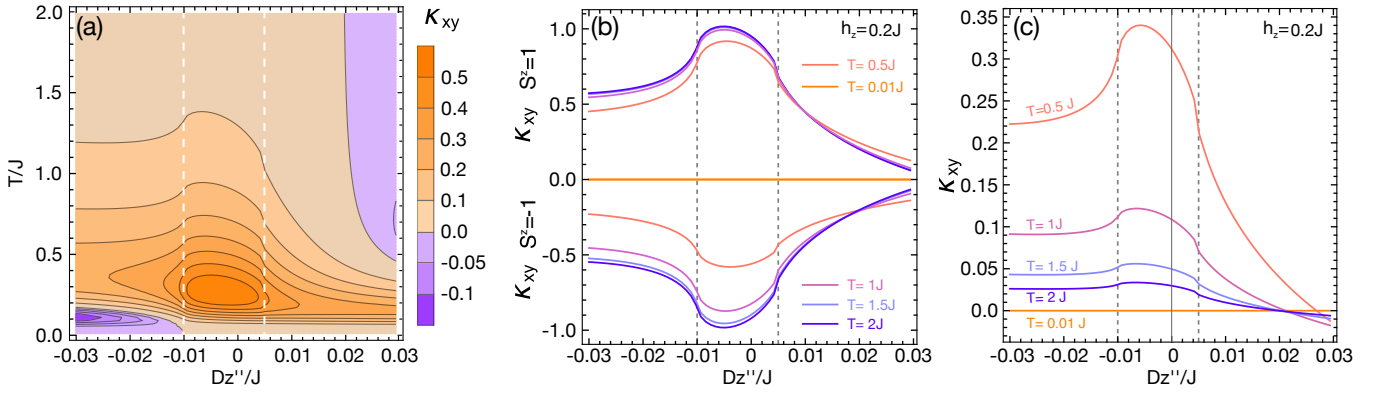


Figure 16: (a) The thermal Hall coefficient for  $h = 0.2J$  along the blue dashed line depicted in the phase diagram of Fig. 9 using the same parameters as in Fig. 13. (b) We show the contributions from the  $+1$  and  $-1$  triplets separately. The  $S^z = -1$  triplet moves up in energy, due to the Zeeman splitting, and thus at low temperatures these bands are less filled than those with  $S^z = 1$ , giving a smaller contribution. At higher temperature this difference shrinks, and the sum of the signals, having opposite sign, cancels as  $T \rightarrow \infty$ . (c) Thermal Hall coefficient at various temperatures as the function of  $D''$ . The dashed vertical lines indicate the phase transitions at  $D'' = -D'$  and  $D'' = D'/2$  respectively, where the thermal Hall coefficient has an inflection point.

for both the linear and quadratic touchings [Section V]. The behaviour of the  $\mathcal{Z}_2$  topological phase is also characterised through calculations of its topological invariant, and the associated triplet Nernst effect [Section VI].

Finally, we explore two different mechanisms which can eliminate the  $\mathcal{Z}_2$  topology of the triplon bands, protected by the  $\text{TR} \times \text{U}(1)$  symmetry. The first route to remove the  $\mathcal{Z}_2$  phase is the breaking of time-reversal symmetry. In applied magnetic field the triplon bands split and the system becomes a Chern insulator, exhibit finite thermal Hall response and chiral modes on open edges [Section VIII], in a straightforward analogy with the Kane and Mele model<sup>7,8</sup>. The second, less trivial route, is the inclusion of bond-nematic interactions, permitted by the symmetry of the lattice, which mixes the triplets with  $m = 1$  and  $-1$ , thereby breaking the  $\text{U}(1)$  symmetry [Section VII].

In contrast to the electronic model of Kane and Mele, where the mixing of states with  $S^z = \pm \frac{1}{2}$  by (weak) Rashba interactions is compatible with a spin-Hall state, these terms have a singular effect, immediately changing the topology of the triplon bands. Such bond-nematic interactions, typically referred to as symmetric exchange anisotropies, are naturally present in other spin models too, proposed to exhibit  $\mathcal{Z}_2$  bands

realized by magnetic excitations. We traced back the difference to the time-reversal breaking properties of the Pauli matrices, representing the  $S^z = \pm 1$  triplets.

The nematic terms and in-plane DM interactions, breaking the  $\text{U}(1)$  symmetry and mixing the spins, can also be present in other models proposed as bosonic analogues of  $\mathcal{Z}_2$  bands, including bilayer ordered magnets<sup>27</sup>, and paramagnets<sup>32</sup>. Our results call for a detailed investigations of the consequences of the various  $\text{U}(1)$  symmetry-breaking terms in bosonic systems in general.

### Acknowledgments

JR gratefully acknowledges discussions with Christian D. Batista. The authors also gratefully acknowledge the hospitality of the KITP program “*Topological Quantum Matter: Concepts and Realizations*”, where a part of the work was carried out. This work was supported by the Theory of Quantum Matter Unit of the Okinawa Institute of Science and Technology Graduate University (OIST), and the Hungarian NKFIH Grant No. K124176. This research was supported in part by the National Science Foundation under Grant No. NSF PHY-1748958.

<sup>1</sup> K. v. Klitzing, G. Dorda, and M. Pepper, *Phys. Rev. Lett.* **45**, 494 (1980).  
<sup>2</sup> R. B. Laughlin, *Phys. Rev. B* **23**, 5632 (1981).  
<sup>3</sup> D. J. Thouless, M. Kohmoto, M. P. Nightingale, and M. den Nijs, *Phys. Rev. Lett.* **49**, 405 (1982).  
<sup>4</sup> J. E. Avron, R. Seiler, and B. Simon, *Phys. Rev. Lett.* **51**, 51 (1983).  
<sup>5</sup> M. Kohmoto, *Annals of Physics* **160**, 343 (1985).  
<sup>6</sup> F. D. M. Haldane, *Phys. Rev. Lett.* **61**, 2015 (1988).  
<sup>7</sup> C. L. Kane and E. J. Mele, *Phys. Rev. Lett.* **95**, 226801 (2005).

<sup>8</sup> C. L. Kane and E. J. Mele, *Phys. Rev. Lett.* **95**, 146802 (2005).  
<sup>9</sup> M. Z. Hasan and C. L. Kane, *Rev. Mod. Phys.* **82**, 3045 (2010).  
<sup>10</sup> X.-L. Qi and S.-C. Zhang, *Rev. Mod. Phys.* **83**, 1057 (2011).  
<sup>11</sup> M. G. Vergniory, L. Elcoro, C. Felser, N. Regnault, B. A. Bernevig, and Z. Wang, *Nature* **566**, 480 (2019).  
<sup>12</sup> M. Onoda, S. Murakami, and N. Nagaosa, *Phys. Rev. Lett.* **93**, 083901 (2004).  
<sup>13</sup> T. Ozawa, H. M. Price, A. Amo, N. Goldman, M. Hafezi, L. Lu, M. C. Rechtsman, D. Schuster, J. Simon, O. Zilberberg, and I. Carusotto, *Rev. Mod. Phys.* **91**, 015006 (2019).

- <sup>14</sup> C. H. Lee, S. Imhof, C. Berger, F. Bayer, J. Brehm, L. W. Molenkamp, T. Kiessling, and R. Thomale, *Communications Physics* **1**, 39 (2018).
- <sup>15</sup> V. Peri, M. Serra-Garcia, R. Ilan, and S. D. Huber, *Nature Physics* **15**, 357 (2019).
- <sup>16</sup> M. Fruchart, Y. Zhou, and V. Vitelli, *Nature* **577**, 636 (2020).
- <sup>17</sup> Y. Onose, T. Ideue, H. Katsura, Y. Shiomi, N. Nagaosa, and Y. Tokura, *Science* **329**, 297 (2010).
- <sup>18</sup> R. Shindou, R. Matsumoto, S. Murakami, and J.-i. Ohe, *Phys. Rev. B* **87**, 174427 (2013).
- <sup>19</sup> A. Mook, J. Henk, and I. Mertig, *Phys. Rev. B* **89**, 134409 (2014).
- <sup>20</sup> A. Mook, J. Henk, and I. Mertig, *Phys. Rev. B* **90**, 024412 (2014).
- <sup>21</sup> S. Owerre, *Journal of Physics: Condensed Matter* **28**, 386001 (2016).
- <sup>22</sup> A. L. Chernyshev and P. A. Maksimov, *Phys. Rev. Lett.* **117**, 187203 (2016).
- <sup>23</sup> V. A. Zyuzin and A. A. Kovalev, *Phys. Rev. Lett.* **117**, 217203 (2016).
- <sup>24</sup> S. K. Kim, H. Ochoa, R. Zarzuela, and Y. Tserkovnyak, *Phys. Rev. Lett.* **117**, 227201 (2016).
- <sup>25</sup> K. Nakata, J. Klinovaja, and D. Loss, *Phys. Rev. B* **95**, 125429 (2017).
- <sup>26</sup> P. A. McClarty, X.-Y. Dong, M. Gohlke, J. G. Rau, F. Pollmann, R. Moessner, and K. Penc, *Phys. Rev. B* **98**, 060404 (2018).
- <sup>27</sup> H. Kondo, Y. Akagi, and H. Katsura, *Phys. Rev. B* **99**, 041110 (2019).
- <sup>28</sup> P. A. McClarty and J. G. Rau, *Phys. Rev. B* **100**, 100405 (2019).
- <sup>29</sup> H. Kondo, Y. Akagi, and H. Katsura, *Progress of Theoretical and Experimental Physics* (2020), 10.1093/ptep/ptaa151, ptaa151, <https://academic.oup.com/ptep/advance-article-pdf/doi/10.1093/ptep/ptaa151/33976880/ptaa151.pdf>.
- <sup>30</sup> J. Romhányi, K. Penc, and R. Ganesh, *Nat Commun* **6**, 6805 EP (2015).
- <sup>31</sup> P. A. McClarty, F. Kruger, T. Guidi, S. F. Parker, K. Refson, A. W. Parker, D. Prabhakaran, and R. Coldea, *Nat Phys advance online publication*, (2017).
- <sup>32</sup> D. G. Joshi and A. P. Schnyder, *Physical Review B* **100**, 020407 (2019).
- <sup>33</sup> P. S. Kumar, I. F. Herbut, and R. Ganesh, *Phys. Rev. Research* **2**, 033035 (2020).
- <sup>34</sup> Y. Akagi, H. Katsura, and T. Koma, *Journal of the Physical Society of Japan* **86**, 123710 (2017), <https://doi.org/10.7566/JPSJ.86.123710>.
- <sup>35</sup> N. Yoshioka, Y. Akagi, and H. Katsura, *Phys. Rev. B* **97**, 205110 (2018).
- <sup>36</sup> R. Cheng, S. Okamoto, and D. Xiao, *Phys. Rev. Lett.* **117**, 217202 (2016).
- <sup>37</sup> H. Katsura, N. Nagaosa, and P. A. Lee, *Phys. Rev. Lett.* **104**, 066403 (2010).
- <sup>38</sup> R. Matsumoto and S. Murakami, *Phys. Rev. B* **84**, 184406 (2011).
- <sup>39</sup> A. L. Chernyshev and M. E. Zhitomirsky, *Phys. Rev. B* **92**, 144415 (2015).
- <sup>40</sup> J. Fransson, A. M. Black-Schaffer, and A. V. Balatsky, *Phys. Rev. B* **94**, 075401 (2016).
- <sup>41</sup> H.-S. Kim and H.-Y. Kee, *npj Quantum Materials* **2**, 20 (2017).
- <sup>42</sup> H. Kondo, Y. Akagi, and H. Katsura, *Phys. Rev. B* **99**, 041110 (2019).
- <sup>43</sup> H. Kondo, Y. Akagi, and H. Katsura, *Phys. Rev. B* **100**, 144401 (2019).
- <sup>44</sup> L. Fu and C. L. Kane, *Phys. Rev. B* **76**, 045302 (2007).
- <sup>45</sup> J. E. Moore and L. Balents, *Phys. Rev. B* **75**, 121306 (2007).
- <sup>46</sup> R. Roy, *Phys. Rev. B* **79**, 195321 (2009).
- <sup>47</sup> S. Sachdev and R. N. Bhatt, *Physical Review B* **41**, 9323 (1990).
- <sup>48</sup> A. Collins, C. Hamer, and Z. Weihong, *Physical Review B* **74**, 144414 (2006).
- <sup>49</sup> B. Simon, *Phys. Rev. Lett.* **51**, 2167 (1983).
- <sup>50</sup> M. V. Berry, *Proceedings of the Royal Society of London. A. Mathematical and Physical Sciences* **392**, 45 (1984).
- <sup>51</sup> T. Fukui, Y. Hatsugai, and H. Suzuki, *Journal of the Physical Society of Japan* **74**, 1674 (2005), <https://doi.org/10.1143/JPSJ.74.1674>.
- <sup>52</sup> M. Oshikawa, *Phys. Rev. B* **50**, 17357 (1994).
- <sup>53</sup> K. Nawa, K. Tanaka, N. Kurita, T. J. Sato, H. Sugiyama, H. Uekusa, S. Ohira-Kawamura, K. Nakajima, and H. Tanaka, *Nature Communications* **10**, 2096 (2019).
- <sup>54</sup> Y. D. Chong, X.-G. Wen, and M. Soljačić, *Phys. Rev. B* **77**, 235125 (2008).
- <sup>55</sup> A. A. Kovalev and V. Zyuzin, *Phys. Rev. B* **93**, 161106 (2016).
- <sup>56</sup> V. A. Zyuzin and A. A. Kovalev, *Phys. Rev. B* **97**, 174407 (2018).

## Appendix A: Time-reversal symmetry

Before we start, let us briefly overview how our pseudo-spin operators behave under time-reversal (TR) symmetry, as well as the notation we will follow. The Pauli matrices,  $\sigma^x$ ,  $\sigma^y$ , and  $\sigma^z$  act in the sublattice, i.e. they represent the pseudo-spin-half formed by the two levels that cross. As the TR symmetry leaves the site indices intact and, therefore, does not affect the levels, the real operators  $\sigma^x$ , and  $\sigma^z$  are TR invariant, while  $\sigma^y$  acquires a minus sign due to the complex conjugation, breaking TR. The Pauli matrices  $s^x$ ,  $s^y$ , and  $s^z$  denote the pseudo-spin-half, formed by the +1 and -1 triplet states. Although these operators stand for the spin degrees of freedom, one has to be careful with their TR breaking properties. The TR operator for the dimer has the form

$$T = e^{i\pi(S_1^y + S_2^y)} \cdot \mathcal{K} = \begin{pmatrix} 1 & 0 & 0 & 0 \\ 0 & 0 & 0 & 1 \\ 0 & 0 & -1 & 0 \\ 0 & 1 & 0 & 0 \end{pmatrix} \cdot \mathcal{K}, \quad (\text{A1})$$

where the basis is  $(|s\rangle, |t_{-1}\rangle, |t_0\rangle, |t_1\rangle)$  and  $\mathcal{K}$  denotes a complex conjugation. Thus the TR operator for the spin-1 formed by the triplets is

$$T = \begin{pmatrix} 0 & 0 & 1 \\ 0 & -1 & 0 \\ 1 & 0 & 0 \end{pmatrix} \cdot \mathcal{K}. \quad (\text{A2})$$

The state  $|t_0\rangle$  changes sign, while the  $|t_1\rangle$  and  $|t_{-1}\rangle$  transform into each other. This can also be shown writing the triplets in their usual form  $|t_1\rangle = |\uparrow\uparrow\rangle$ ,  $|t_{-1}\rangle = |\downarrow\downarrow\rangle$ , and  $|t_0\rangle = \frac{1}{\sqrt{2}}(|\uparrow\downarrow\rangle + |\downarrow\uparrow\rangle)$ , and using that the TR acts on the spin-half as  $T : |\uparrow\rangle \rightarrow |\downarrow\rangle$ , and  $T : |\downarrow\rangle \rightarrow -|\uparrow\rangle$ .

Restricting ourselves to the up and down triplet states, and considering them as the components of a pseudo spin-half, the Pauli matrices formed by them will transform differently under TR than those of a real spin-half (where all of them break TR). The TR acts on the pseudo-up and down spins as  $T : |1\rangle \rightarrow |-1\rangle$ , and  $T : |-1\rangle \rightarrow |1\rangle$ . Therefore, among the

Pauli matrices

$$s^x = |1\rangle\langle -1| + |-1\rangle\langle 1| \quad (\text{A3a})$$

$$s^y = -i|1\rangle\langle -1| + i|-1\rangle\langle 1| \quad (\text{A3b})$$

$$s^z = |1\rangle\langle 1| - |-1\rangle\langle -1|, \quad (\text{A3c})$$

the  $s^x$  and  $s^y$  are invariant under TR, and  $s^z$  remains the only TR breaking operator. This is an important difference between the pseudo-spin-half formed by the triplets  $|1\rangle$  and  $|-1\rangle$ , and the real spin-half of an electron, for example.

### Appendix B: $\mathcal{Z}_2$ invariant from the parity eigenvalues

band		bottom	middle	top
parity eigenvalue	$\xi_m(\Gamma)$	1	1	1
	$\xi_m(M_1)$	-1	1	-1
	$\xi_m(M_2)$	1	-1	1
	$\xi_m(M_3)$	1	-1	1
$\mathcal{Z}_2$ index	$\nu$	1	0	1

Table II: Parity eigenvalues of the bottom (black), middle (purple) and, top (red) bands for each spin degree of freedom,  $m$  at the time reversal invariant momenta,  $\Gamma_i$ .

In an inversion symmetric system, the  $\mathcal{Z}_2$  can be easily calculated using the parity eigenvalues at the four time-reversal invariant momenta (TRIM)<sup>44</sup>.

$$\prod_{i=1}^4 \xi(\Gamma_i) = (-1)^\nu. \quad (\text{B1})$$

The TRIM,  $\Gamma_i$  correspond to  $\Gamma$ ,  $M_1$ ,  $M_2$ , and  $M_3$  shown in Fig. 1(a) of the main text. When the product is  $-1$ , the exponent  $\nu$  is odd and the system is topologically nontrivial. For even  $\nu$  values the system is trivial.

We define the parity operator ( $\mathcal{P}$ ) as the inversion through the center of the dimer  $A$ . Consequently, the effect of  $\mathcal{P}$  on dimer  $A$  is the exchange of its sites 1 and 2, while dimer  $B$  will also be shifted by  $\delta_y$  and dimer  $C$  by  $\delta_x$  from their original positions beside exchanging their sites (see Fig. 1 in the main text).

Changing the site indices, 1 and 2 does not affect the triplets, which are even under permutation, nor has the inversion any effect on the spin degrees of freedom. Thus,  $\mathcal{P}$  will not mix different  $m$  bands and we can treat each sector separately again. In momentum space  $\mathcal{P}_m$  becomes diagonal,

$$\mathcal{P}_m = \begin{pmatrix} \underline{t}_m^\dagger(\mathbf{k}) \\ \underline{t}_{-m}^\dagger(-\mathbf{k}) \end{pmatrix} \begin{pmatrix} P_{\mathbf{k}} & \mathbf{0} \\ \mathbf{0} & P_{\mathbf{k}} \end{pmatrix} \begin{pmatrix} \underline{t}_m(\mathbf{k}) \\ \underline{t}_{-m}^\dagger(-\mathbf{k}) \end{pmatrix} \quad (\text{B2})$$

where

$$P_{\mathbf{k}} = \text{diag}(1, e^{i\delta_y \cdot \mathbf{k}}, e^{i\delta_x \cdot \mathbf{k}}) \quad (\text{B3})$$

We compute the eigenvectors of  $\mathcal{H}_m$  numerically at each TRIM,  $\Gamma_i = (\Gamma, M_1, M_2, M_3)$ , and determine their eigenvalue,  $\xi_m(\Gamma_i)$  with  $\mathcal{P}_m$  defined in Eq. (B2). When inversion symmetry is present, the  $\mathcal{P}_m$  commutes with  $\mathcal{H}_m$  at the TRIM. The parity eigenvalues of the bands are collected in Table II. The  $\mathcal{Z}_2$  indices of the bottom and top bands are 1, while it is 0 for the middle band. Let us note that if we chose dimer  $B$  as the center of inversion, the parity eigenvalues for the point  $M_2$  would become  $-1$ ,  $1$ , and  $-1$ , while  $\xi_m(M_1)$  and  $\xi_m(M_3)$  would be  $1$ ,  $-1$ , and  $1$ . Similarly, setting dimer  $C$  as the inversion center results in a further cyclic permutation of the rows of Table II. This corresponds to the three-fold symmetry of the  $ABC$ -triangles.